Journal of Ceramic Processing Research. Vol. 21, No. 2, pp. 170~191 (2020)
(Received 7 October 2019, Received in revised form 12 December 2019, Accepted 24 December 2019)
https://doi.org/10.36410/jcpr.2020.21.2.170

J O U R N A L O F
Ceramic Processing Research

Carbon nanotube-biomorphic composites and filter application: A Review

Jung Gyu Park[a], Se Young Kim[b], In Sub Han[b] and Ik Jin Kim[a,*]
[a]*Institute for Processing and Application of Inorganic Materials, (PAIM), Department of Materials Science and Engineering, Hanseo University, 46, Hanseo 1-ro, Haemi-myun, Seosan-si, Chungnam, 31962, Korea*
[b]*Korea Institute of Energy Research (KIER), 152, Gajeong-gu, Daejeon, 34129, Korea*

As interest in environmental pollution has increased, research in the field of filtration has been concentrated. While various types of filters have been developed, research on nanomaterial filtration has been limited. Since then, the development of new materials such as carbon nanotubes (CNTs) has accelerated the study of new filters. Especially, CNTs have been among the most attractive materials ever synthesized for the development of nano-technologies. However, there are fundamental technical problems to be solved the development of new CNT composites. One of these problems is the development of a CNTs filter with excellent adsorption behavior and a filter that is capable of filtering a specific substance. In addition, it is necessary to develop a technology to increase the uniform distribution of CNTs, and to reduce the high processing cost of CNT composite production. In general, the chemical pathways for the production of CNTs include hydrocarbon gases, such as methane (CH_4) and acetylene (C_2H_2), through metal nanoparticle catalysts. However, nano-metal particles have a strong coagulation phenomenon at high temperature by catalytic chemical vapor deposition (CCVD) method. In this review, attempts were made by applying three different reaction techniques to form CNTs on biomorphic carbon materials (BCM) coated with catalyst materials to control the shape and size of CNTs. Hierarchical carbon substrates with pore size of 100 ~ 300 μm were developed using carbonization reaction. Linde type A (LTA) zeolite, silicalite-1, and mesoporous SiO_2 template crystals were simultaneously synthesized and coated on the BCM by an *in-situ* hydrothermal process to synthesize high-yield CNTs composites.

Key words: Carbon nanotubes, Template, Biomorphic carbon materials, Catalytic chemical vapor deposition, Nanofilters.

1. Introduction

Recently, there has been increased interest in approaches used for the production of various hierarchical and complex microstructures with biodiversity-carbon materials with natural biological substances, such as wood [1], rattan [2], or rice husk [3] used as a template. Of these, natural trees have received considerable attention, as their cell structure is so large that their tissue structure is converted into a template material [4, 5]. Biomorphic materials with unique and elaborate structures can be obtained by the pyrolysis of tree varieties such as *Chamaecyparis obtusa* (Cypress, a.k.a. Hinoki), *Pinus resinosa*, and *Picea* [6], resulting in carbonaceous forms. This form produces a steel and ceramic mold complex that can penetrate and react with coated oxides and non-oxides to be used in a wide range of applications, such as filtration and catalysts for potentially powerful technical applications. Because of the wide range of applications, it is very important to produce sufficient quantities of well-defined and organized carbon nanotube (CNT) arrays at low cost [7, 8].

*Corresponding author:
Tel : +82 41 660 1441
Fax: +82 41 660 1441
E-mail: ijkim@hanseo.ac.kr

Recent reports of CNT composites research of medical, energy storage, and filtration applications [9-12] due to their morphological, physical, and chemical properties have been published [13, 14]. The high efficiency of CNT in filtration can be explained by observing the structure in which high surface area and large aspect ratio lead to the formation of strong Van der Waals forces between individual CNTs. This is because the microbial cytotoxicity of CNTs partially affects the filtration performance, which has a larger pore size that can fix contaminants, including bacteria and viruses, in flocculation and interstitial pore spaces [15, 16]. The use of such nanomaterials embedded in membranes or other structural media has been considered an effective method for more approaches than just water treatment. The dense CNTs network, which forms a variety of pore sizes from micropores to medium pores supported on ceramic substrates, can be used to physical adsorbents for removing contaminants [17], which make them advantageous for filters in gas adsorption, and water filtration and purification systems [18-20] Other applications include hydrocarbon separation [21], and polluted air filters [22].

All these characteristics provide fundamentally different opportunities for the development of new CNT-containing composites however, several technical challenges were remained. One of them is a CNT oil filter with excellent

adsorption behavior, and a suitable filter to convert it to a filter that is suitable for a specific application. In addition, the producing of CNTs composites has a number of technical problems that need to be addressed. These include the potential damage to CNTs in the substrate; it has been found to be an important and difficult challenge to obtain a uniform and un-agglomerated distribution of CNTs in the matrix, also is the high cost of processes associated with CNTs and their composites.

The chemical pathway for CNTs production is the decomposition of hydrocarbon gases through metal nanoparticle catalysis using metals such as cobalt (Co), iron (Fe), nickel (Ni), and copper (Cu). However, as the CNTs size decreases to nanoscale, the metal particles agglomerate strongly during the synthesis of CNTs at high temperatures. Thus, with respect to template-coated porous ceramics and nanostructured biomorphic carbon materials (BCM), it is desirable to maintain the shape and size of the CNTs at chemical vapor deposition (CVD) treatment temperatures of 650 ~ 750 ºC, as they are required to homogeneously penetrate carbon sources like methane (CH_4) and acetylene (C_2H_2) [23-25].

Generally, matrices or catalyst supports such as alumina [26], mesoporous silica [27], and zeolite [28], have been used to prevent the agglomeration of the catalyst nanoparticles. Among them, zeolites are considered an excellent template for the support or encapsulation of catalyst nanoparticles, because of their well-defined pore structure, and high surface area [29], thereby leading to a catalyst-particle stabilization, the production of a fine dispersion of nanoparticles, and the increase of the number of nucleation sites, which is advantageous for high-yield CNTs synthesis [30, 31].

This review summarizes the formation of CNTs in a template coated BCM using the catalytic chemical vapor deposition (CCVD) method. The synthesis was carried out with the application of a three-step processing route for CNTs composites. First, a BCM was produced by a carbonizing reaction. Secondly, the templates were synthesized within and coated simultaneously on the carbon template using the *in-situ* method and wet process. The BCM was then subjected to a wetting process that resulted in the formation of a metal-ion loaded template; and finally, the CNTs were synthesized using the CCVD method.

Carbon Nanotubes

In the mid-1980s, Kroto et al. (1996 Nobel Prize in Chemistry) discovered a new closed carbon form that consisted of hexagonal and pentagonal faces (buckminster-fullerene-C60). Most notable is the discovery of one-dimensional (1D) CNTs and two-dimensional (2D) single atomic layer carbon, graphene (Nobel Prize 2010) [32]. An important feature of this carbon material has attracted a large number of researchers to explore its unique properties for various engineering topics, and to develop new applications. CNTs was first discovered by Dr. Sumio Iijima as a needle-shaped tube composed of "coaxial tubes of graphite sheets" and has been cited more than 10,000 times in almost all articles on CNTs to date [33].

Types of carbon nanotubes

The ability to combine in different ways is a unique feature of carbon that creates multiple homogeneous forms. If the four atoms of the carbon atom are equally shared (sp^3 hybridization), a diamond will form Fig. 1. Graphite can be changed from diamond to diamond, and from fullerene to CNTs and graphene. When three electrons are shared in one plane and the fourth electron is localized (sp^2 hybridization) between all the atoms, graphite is formed [34, 35]. This type of bond shows a very strong bond; but in graphite, the graphene layer is weak, with van der Waals bond. Carbon, also called fullerene, is another overlapping graphene sheet of sp^2-bonded carbon atoms Fig. 1(b). These nanotubes are concentric graphitic cylinders capped at either end by a half fullerene, owing to the presence of five membered rings. Depending on the number of carbon sheets, these nanotubes can be classified into two types: single-walled CNTs (SWCNTs) and multi-walled CNTs (MWCNTs) with double-walled CNTs (MWCNTs), as shown in Figs. 1(c) and (d).

SWCNTs have a small diameter of 0.4 ~ 4 nm and exhibit a certain property that can be metallic or semi-conducting, depending on their chirality [36]. On average, without chirality control, one-third of metallic and two-thirds of semi-conducting SWCNTs can be obtained. A SWCNTs is considered perfectly crystalline, that is defect-free, if the grapheme sheet has no variations in the hexagonal aromatic structure of the carbon atoms [37].

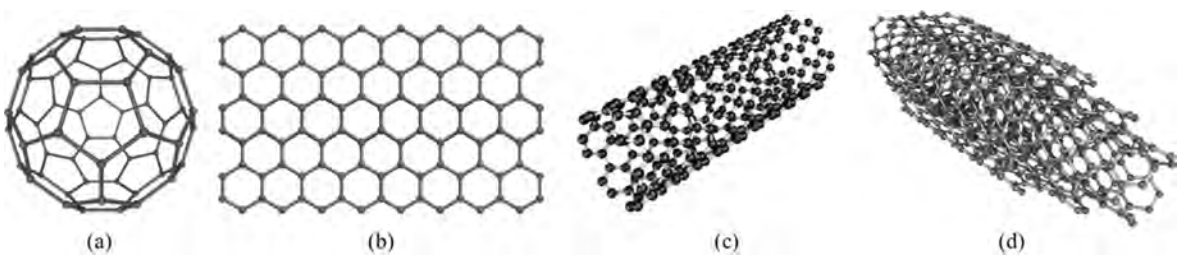

Fig. 1. Illustration of ideal (a) fullerene, (b) graphene, and (c) SWCNT and MWCNT (all cited from Wikimedia Commons).

MWCNTs can be visualized as concentric SWCNTs, which have several walls ranging from two to less than a hundred, leading to the diameter of a MWCNT ranging from 1 nm, and rarely reaching over 100 nm. In MWCNTs, the general innertube distance is 0.34 nm, which is the same distance as that between two parallel graphene sheets in the graphite. Given the ratio of metallic to semi-conducting is 1/3 to 2/3 for SWCNTs, it can be expected that MWCNTs are metallic, in that at least one of the walls will be metallic. Some teams have been able to grow monochiral MWCNTs, indicating that all walls have the same chirality [38, 39]. Ideally, crystalline SWCNTs and MWCNTs have walls and caps without any defects, i.e. missing or added atoms, which are extremely difficult to attain with our current synthesis techniques, and to properly characterize. To date, some teams have grown individual or strands of CNTs with a length of a few centimeters [40].

Properties and application of CNTs

As mentioned previously, depending on the chirality, SWCNTs can be metallic or semi-conducting. Due to this unique structure, SWCNTs have been studied in focus. The degree of twist of the graphite sheet is characterized by a pair of vectors (n, m), which are called chiral vectors, where the integers n and m represent the number of unit vectors along two directions in the honeycomb crystal of graphene [41], as shown in Fig. 2. Because of the varying degrees of twist of their rolled graphite sheets along the length, CNTs can have a different chiral structure. In case of, m = 0, the nanotubes are called "zigzag structure"; if n = m, these nanotubes called "armchair structure"; other nanotubes are called "chiral structure". In addition, if (n – m) of the chiral vector is a multiple of 3, SWCNTs exhibit a metallic behavior; if (n – m) is not a multiple of 3, it exhibits a semi-conducting behavior. This is due to the change in density of the Fermi energy state. Also depending on their diameter and the helicity of the arrangement of graphite rings in the walls, they have been demonstrated to possess unique electronic, photonic, magnetic, thermal, and mechanical properties. Due to their unique physical and chemical properties [42], Nanotubes are being used in a wide range of applications, such as nano-electronic devices [43], interconnects [44], sensors and actuators [45], energy storage media [46], and field emitters [47] et al.

Theoretical studies have suggested that the ideal CNTs are ballistic conductors for distances in the order of a micron [48]. The 1D confinement of electrons combined with the requirements for energy and momentum conservation leads to ballistic conduction. The electrical properties of SWCNTs have been studied intensively [49], often for the purpose of developing devices such as interconnects [50] or CNTs-based transistors [51]. In contrast, the electrical properties of MWCNTs have not been investigated at the same level of detail, due to their additional complexities arising from the structure, as every shell has different electronic characteristics and chirality, besides the interactions

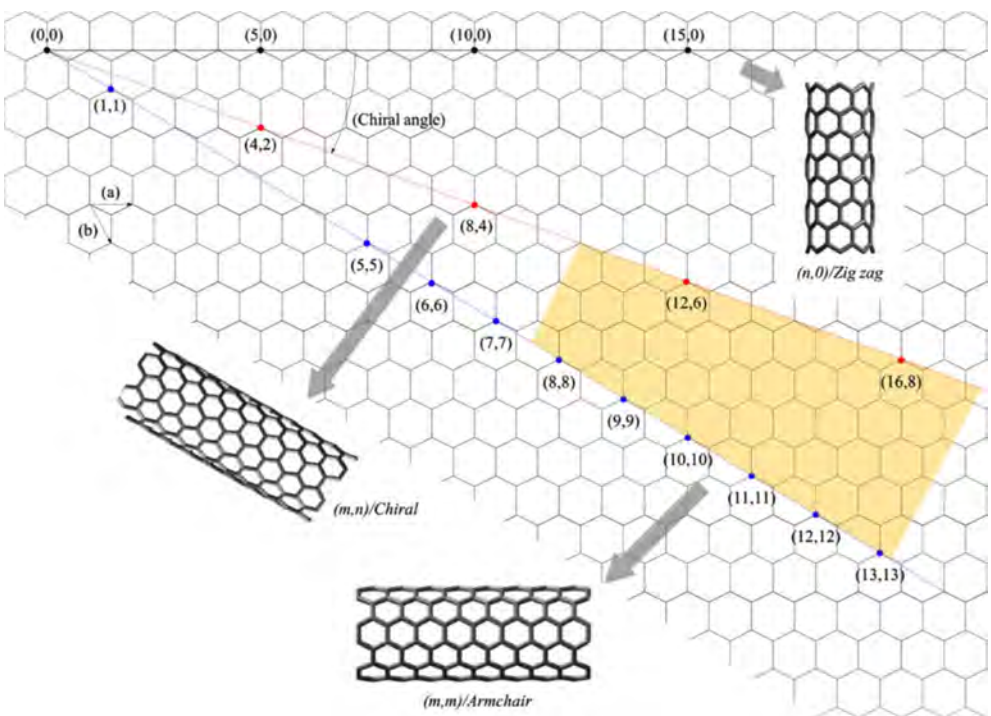

Fig. 2. Chirality (θ) of SWCNTs derived by rolling the Hamada vector of the graphene sheet ((Reproduced from ref. 8, Copyright 2012 Springer).

Table 1. The mechanical and thermal properties of CNTs.

Property	Carbon nannotube
Specific gravity	0.8 g/cm^3 for SWCNT 1.8 g/cm^3 for MWCNT (Theoretical)
Elastic modulus	Up to 1 TPa for SWCNT 0.3 to 1 TPa for MWCNT
Strength	50 to 500 GPa for SWCNT 10 to 60 GPa for MWCNT
Resistivity	5 to 50 μΩcm
Thermal conductivity	3000 Wm^{-1}K^{-1} (Theoretical)
Magnetic susceptibility	22×10^6 EMU/g (Perpendicular with plane) 0.5×10^6 EMU/g (Parallel with plane)
Thermal expansion	Negligible (Theoretical)
Thermal stability	> 700 ºC (in air) 2800 ºC (in vacuum)
Specific surface area	10 to 20 m^2/g

between them [52].

However, for MWCNTs with both ends connected by metallic contacts, electronic transport is dominated by outer-shell conduction at low temperature and bias [53]. Theoretical models and experimental results point to the critical role of shell-to-shell interactions to significantly lower the resistance of MWCNTs with a large number of walls [54, 55]. Theoretical calculations [56] and experimental results [57] indicate that CNTs are stiffer than diamond, exhibiting the highest Young's modulus and tensile strength. Since CNTs are rolled-up graphene sheets, a first approximation for their elastic modulus would be that of graphene, being approximately 1,000 GPa, five times that of steel. Many experiments have confirmed the theoretical predictions. For example, Yu et al. [58] measured the CNTs tensile load using Atomic Force Microscopy (AFM), and found Young's modulus values ranging 320 and 1,470 GPa (average 1,002 GPa), which is consistent with the value estimated by Krishnan et al. [59] based on the observations of SWCNTs freestanding room temperature vibrations in transmission electron microscopy (TEM). Using first-principles calculations, Zhou et al. [60] estimated the Young's modulus of 760 GPa and tensile strength of 6.2 GPa for SWCNTs, while molecular dynamics studies by Yao et al. [61] led to values of 3.6 GPa for Young's modulus, and of 9.6 GPa for tensile strength. Using TEM, Demczyk et al. [62] measured a Young's modulus of 0.9±0.18 TPa and a tensile strength of 150 ±45 GPa, which are comparable to those of graphene sheets.

Innertube coupling in SWCNTs and inter-shell coupled MWCNTs result in a low-temperature specific heat that resembles that of 3D graphite [63]. Pop et al. reports the thermal properties of a suspended metallic SWCNTs were extracted from high-bias (I-V) electrical characteristics achieved by Joule self-heating over the 300 ~ 800 K temperature range [64]. They measured a thermal conductivity of almost 3,500 $Wm^{-1}K^{-1}$ at room temperature (RT) for a 2.6 mm length of SWCNT with a diameter of 1.7 nm and developed a model of thermal conductivity as a function of nanotube diameter and temperature. Similarly, Kim et al. [65] measured a thermal conductivity above 3,000 $Wm^{-1}K^{-1}$ at RT for MWCNTs using a microfabricated suspended device. The property of field emission relates to the extraction of electrons from a solid material by tunneling through the surface potential barrier. The emitted current depends directly on the local electric field at the emitting surface and its work function. The Fowler-Nordheim model [66] shows an exponential dependence of the emitted current on the local electric field and the work function. Given that the emitter shape (geometric field enhancement) and the chemical state of the surface have a strong impact on the emitted current, the small diameter and elongated shape of CNTs lead to a high geometrical field enhancement, making them ideal candidates for field emission applications, such as displays or triodes [67]. Another promising field of CNTs is nanostructure-based solar cells [68]. The dispersion of CNTs in a solution of an electron donating conjugated polymer is perhaps the most common strategy to implement CNT materials into organic photovoltaic devices to obtain higher efficiency. It has been reported that enhancements of more than two orders of magnitude have been observed in the photocurrent from adding the SWCNTs to the poly (3-octylthiophene) matrix [69]. As is well known, CNTs have 1D and wire-like structure, making them better at forming electron- or hole-transporting highways in the cell, and their large surface area enhances the separation of the electron-hole pair, leading to conductivity several times greater than that of conducting polymers. In these cells, they can act as both electron donors and acceptors, depending on the redox properties of the other component. The use of CNTs in dye-sensitized solar cells has achieved double efficiency of this kind of photoelectrochemical solar cell [70].

Fabrication method of carbon nanotubes

The most common method for synthesizing CNTs is as follows:

1) Arc-discharge [71-74]
2) Laser ablation [75-77]
3) Chemical vapor deposition from hydrocarbons (CVD) [78-82].

Techniques such as arc discharge and laser ablation enable the synthesis of non-substrate CNTs with good crystallinity at high temperatures. This simple method is the most widely used technique for synthesizing CNTs without a substrate. The choice of the most suitable synthesis method depends on the properties and possibilities required. Therefore, much research is underway to increase yield and efficiency to reduce current production costs. Mass production capability is key to using CNTs in

composites. Compared with CVD processes, arc discharge and laser cutting methods are costly, while CVD is the most suitable technique for scale-up. In order to use CNTs in composites, large quantity production capacity is the key [83]. Therefore, this research will mainly focus on the CVD method.

Electric-Arc discharge

Arc discharge, a method developed by Kratschmer et al. [73], was the first available method for mass-producing both SWCNTs and MWCNTs. This technique has been used initially for fabricating carbon fibers and fullerenes, which may be the reason for CNTs not being characterized, even though they were produced before 1991. For example, Roger Bacon synthesized "thick" carbon whiskers in the early 1960s, as mentioned by Yakobson and Smalley [74]. One can imagine that if he had a HRTEM, he could have found CNTs in the soot. In this technique, CNTs produced by striking an arc electrodes in an inert atmosphere (e.g., He or Ar). If a catalyst is added to one of the electrodes, they can be easily obtained. The mechanism is based on energy transfer between the target material, graphite, which is kept at temperatures close to its melting point, and an external radiation source, as shown in Fig. 3. The technique has a major advantage, in that it is possible to produce CNTs with good crystallinity by tuning the parameters, which leads to their superior electrical and mechanical properties. This may be caused by the high temperature where the process operates, even higher compared to CVD. The major drawback is that CNTs products have to be separated from other carbon products and catalyst residue.

Laser ablation

This method was first introduced by Smalley's group [75] and was used for the production of fullerene clusters. The principle and mechanism of this technique are similar to the arc-discharge technique, but the difference is that the graphite pellets containing the metal-ion catalyst (e.g., Ni or Co) are strike by a laser to generate clusters. Pulsed or continuous laser irradiation to species for vaporizes the carbon and catalysts. The vaporized species are led to a water-cooled collector by a flow gas, where they condense, as shown in Fig. 4. Using this method, MWCNTs can be collected in the soot with diameter of 1.5 to 3.5 nm, and with length of up to 300 nm [76, 77]. The function of the reaction temperature (1,200 °C is optimum temperature for the best quality of CNTs. By introducing small quantities of metal catalyst in the pellet, SWCNTs can be achieved with good crystallinity. Unfortunately, this technique has disadvantage for economic issues, because the process involves high-purity graphite rods, the higher laser powers was required and the amount of CNTs that can be manufactured per day is not as high as for the arc discharge method.

Chemical vapor deposition (CVD)

Chemical Vapor Deposition (CVD) is a commonly used method for the manufacture of thin films and is very different from the two methods mentioned above in the synthesis of CNTs. CVD has the low set-up cost, easy control of experimental parameters, simple synthesis conditions and easy to scale-up to mass production make it one of the most widely used methods of CNTs in recent years. CVD methods can be classified into various methods such as plasma-enhanced CVD and thermal CVD etc. In particular, Catalytic CVD (CCVD), which is a CVD with catalytic pyrosis of hydrocarbon, is applied to the synthesis of CNTs, which enables high yield of nanotubes [78, 79]. This technique provided various advantages over other techniques, where CNTs are grown over metal-ion catalysts containing nanoparticles of transition metals (e.g., Ni, Fe, Co, Cu) or related oxides by the decomposition of a various carbon source (e.g., CH_4, C_2H_2, etc.) [80-82]. Previously, while most CVD-grown CNTs were "spaghetti-like" and defective,

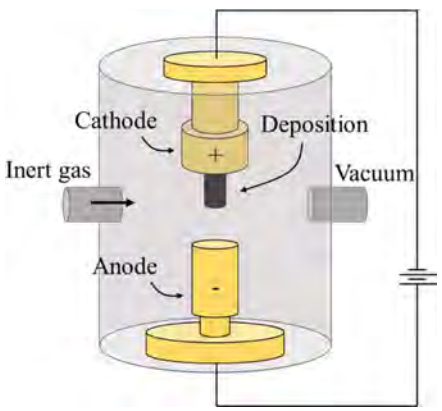

Fig. 3. Schematic diagram of electric-arc discharge apparatus (Reproduced from ref. 8, Copyright 2012 Springer).

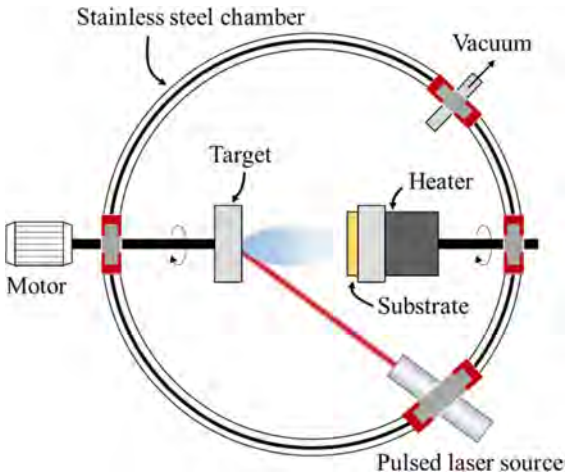

Fig. 4. Schematic diagram of laser ablation apparatus (Reproduced from ref. 8, Copyright 2012 Springer).

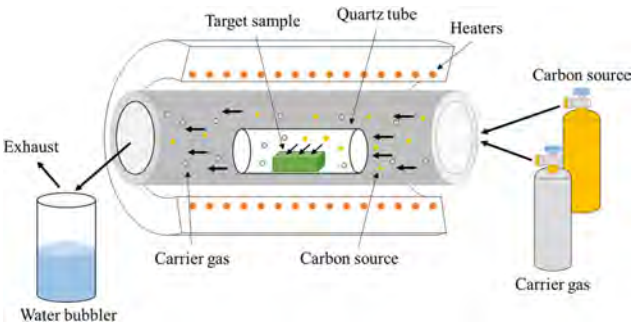

Fig. 5. Schematic of CNTs production by CCVD (Reproduced from ref. 8, Copyright 2012 Springer).

the potential of the method to satisfy technological requirements was recognized. Since 1998, substantial and rapid progress has been made in the development of CVD to establish it as a highly controlled technology for producing CNTs. To date, it is possible to fabricate high-quality SWCNTs and MWCNTs in bulk, or directly onto substrates as a raw material [83-85]. In addition, it can be integrated as a step-in chip fabrication, and by appropriate patterning, can be used to synthesize CNTs in required locations on substrates, although a complete understanding of the growth mechanism of CNTs is still unclear at this time. Fig. 5 shows the synthesis techniques that we used.

Biomorphic Carbon Materials

To apply nanostructures is one of the driving forces of material development. The possibility of controlling the microstructure complexity and interfacial and interconnectivity of microstructural units is a key technology for producing new materials with improved multifunctional properties. Recent research activities have addressed the question of how to transform hierarchical cellular structures of trees to provide specific functional properties [86-89]. Due to the genetic evolution process, biological structures exhibit excellent strength in low density, high stiffness and elasticity, and are resistant to micro damage, as well as at the macroscopic scale. Wood is a natural compound with cellulose, hemicellulose, and lignin as major biopolymeric components and additional macromolecular compounds. Carbonized wood is being used in a wide range of industries as the demand for charcoal increases with the growth of the metal industries.

Recently, carbonized wood has been used as activated carbon in a variety of applications, such as fibers, composites, filters, and catalyst supports [90]. As the importance of the fine chemical industry grows, there is much interest and research in the micro reactor process using activated carbon supported precious metal catalysts [91]. The carbon support may be prepared in powder, pellet, or honeycomb form, and is used as a catalyst filter support or absorbent. Catalysts such as Cu, Pt, Ir, Ru, Pd, Rh, or Mn can be applied, and are used for the thermocatalytic decomposition of methane for hydrogen production, without low temperature selective catalytic reduction NO or CO_2 [92]. However, carbonized wood is more difficult to commercialize, because it has a lower specific surface area (SSA) than commercial activated carbon of 400 ~ 1,200 m^2/g [93]. Mohan et al. [94] obtained carbonized wood with SSA values of 2.04, 2.73, 25.4, and 1.88 m^2/g by carbonizing oak, pine, oak bark, and pine bark at 400 ~ 450 °C, respectively. A recent breakthrough is Yao et al. [95], who carbonized bamboo, sugar barge, and hickory wood at 600 °C, and obtained SSA values of 234, 375.5, 388.3, and 401.0 m^2/g, respectively, under optimized heat treatment conditions [96].

In addition, in the case of interconnected biomimetic structures, it is still a technical challenge to produce CNTs-inserted complexes in all directions. Open pore matrix composites, which are used as trusses depending on the degree of porosity and the degree of filling with nanotubes, can be applied as multifunctional engineering composites, such as filters. CNTs has received special attention, because it has excellent water treatment ability to filter organic and inorganic pollutants [97, 98]. CNT-reinforced composite materials can also potentially improve their mechanical properties.

Wood structure and composition

According to Ramirez-Rico et al. [99], the structure of wood can be roughly divided into two groups for soft- and hardwood, according to its microstructure and composition. The composition of the cell walls is determined by the nature of the wood and the wood-derived product, as shown in Fig. 6 [100]. This can be described as a lamellar or layered microstructure, in which each layer is composed of cellulose, hemicellulose, and lignin (lignocellulose). Cellulose is usually a long polymer chain (up to 1 μm long), agglomerated with microfilaments aligned with the longest dimension of the cell. Hemicellulose is a short chain connecting cellulose microfilaments, and lignin occupies the space left by the cellulose and hemicellulose chains [99, 101, 102]. In addition to the presence of pores and cells, the tree also shows two types of macrostructures: light rays, and growth rings. Light rays are horizontally aligned cells that are used for nutrient storage, and are released in three axes, while growth rings are concentric circles that change pore size, due to seasonal changes in tree growth. Since there is no fluid pathway, the softwood of gym plants, such as conifers, is generally referred to as non-porous, while the hardwood of pizza plants is classified as porous, semi-circular, or porous, depending on the shape of the growth rings [103, 104].

Carbonization and pyrolysis

Pyrolysis of wood to produce a carbon support biomorphic carbon materials (BCMs) by slowly heat up to a temperature above 800 °C with the natural

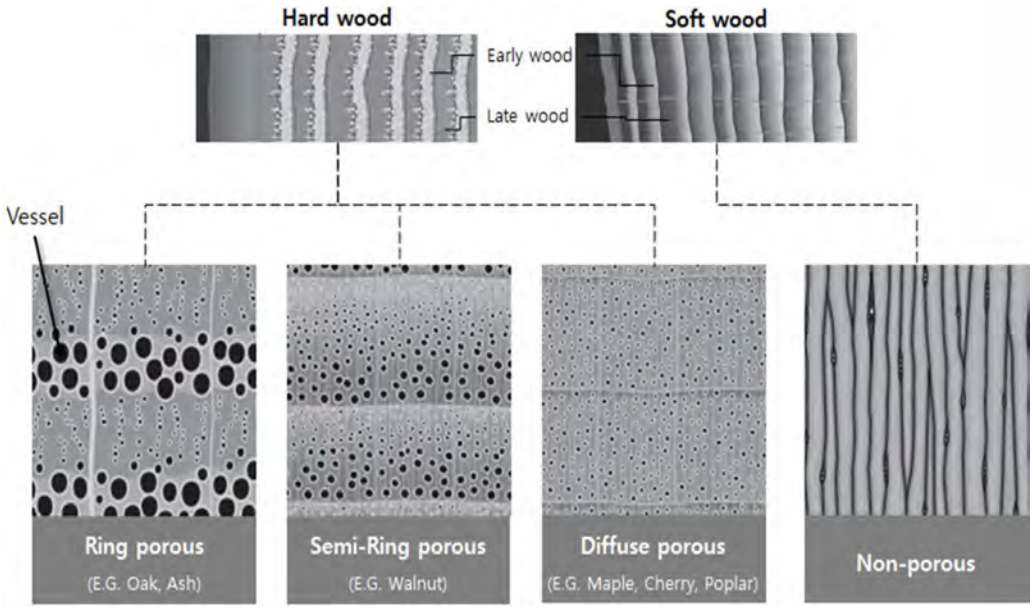

Fig. 6. Axial sections of wood structure from ring porous hardwood and non-porous softwood (Modified from T. Nunlist, Popular Woodworking, Dec. 2012.).

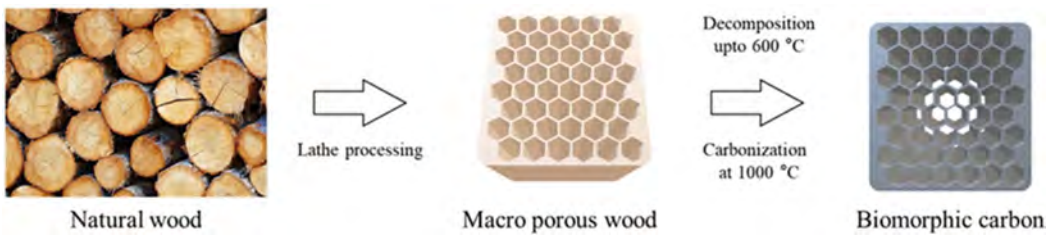

Fig. 7. Carbonization process of natural wood.

wood precursor in an inert atmosphere (typically Ar or N_2). In the pyrolysis process, the other polymer components of the wood decompose hemicellulose at 200 ~ 260 °C and decompose cellulose at 240 ~ 350 °C and lignin at 280 ~ 500 °C, stepwise [105]. In this work, to avoid collapse of the specimen structure during the carbonization process, the specimens were slowly heated in N_2 gas flow 10 cm^3/min in a horizontal electric furnace at a heating rate of 0.5 °C/min to 600 °C for 6 ~ 8 h. Subsequently, the temperature was raised to 1,000 °C at a rate of 3 °C/min to obtain a porous carbon template.

Fig. 8 shows that H_2O, carbonyl groups, CO_2 acids, and alcohols are released, due to degradation of the biopolymer structure at temperatures up to 600 °C during pyrolysis. On the other hand, the major biopolymer components of the cell wall material are rearranged, and converted to carbon struts. Upon thermal decomposition at the initial stage ($T \leq 250$ °C), evaporation of water and decomposition of CO and CO_2 begins with a weight loss of 15 ~ 20%, and then the wood structure breaks CO, H_2, CO_2, and changes into charcoal having about 30% tar between 300 and 500 °C with a weight loss of almost 80%. Fig. 9 shows

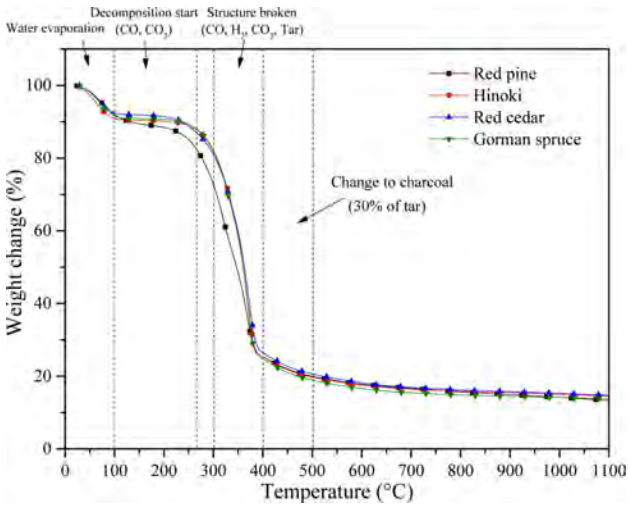

Fig. 8. TGA curves of carbonized biomorphic carbon template from red pine, Cypress, Red cedar, and Gorman spruce.

the microstructure of the axial cross-section of the biomimetic carbon material from pyrolysis of several different precursors used as the base substrate for CNTs synthesis. In all cases, the unique anatomical characteristics

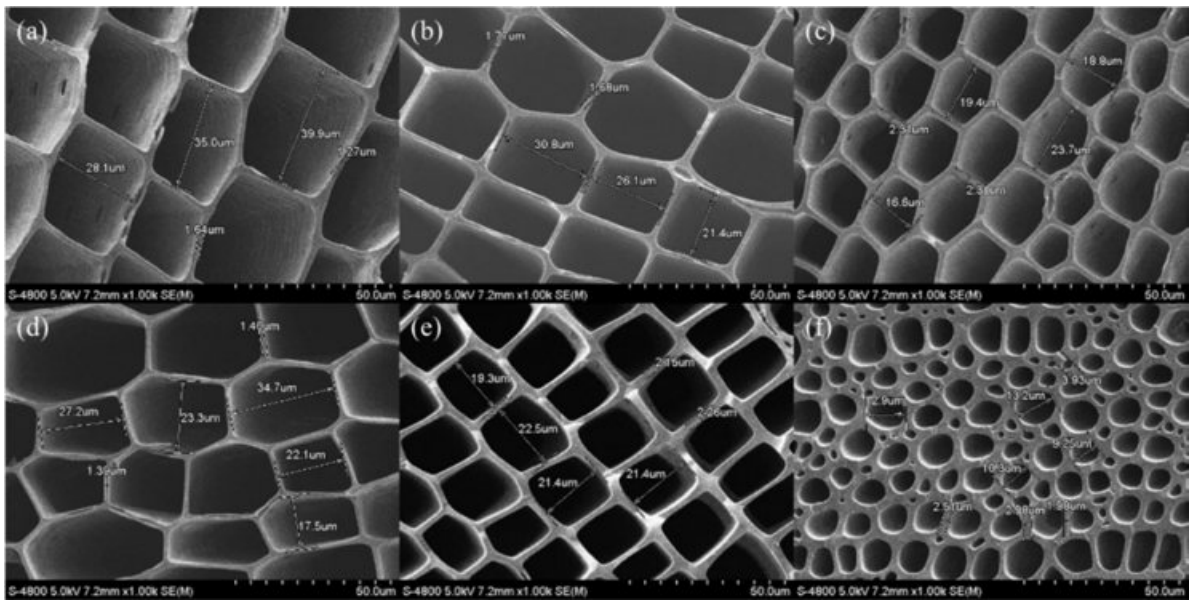

Fig. 9. Macrostructure of hinoki (a), red cedar (b), north american red pine (c), red pine (d), Gorman spruce (e) and Mahogany (f) (Reproduced and modified with permission from ref. 5, 107 and 156, Copyright 2018 Hanyang University and Inderscience publishers).

of the tissue can be maintained during pyrolysis, producing porous materials that are composed mainly of honeycomb and ring-porous carbon structures [106]. It is also clear that after pyrolysis, the pore shape and distribution of the original wood are preserved.

Fig. 9(a) and (b) show a hexagonal cell structure, in which the microstructure of hinoki and red cedar has a pore size (long side *) in the range 18.8 to 23.7 μm, while each cell wall thickness is of about 2.30 ~ 1.40 μm. Fig. 9(c), (d), and (e) show the microstructure of North American red pine, red pine, and Gorman spruce with a rectangular cell, and square structure with pore size ranging 19.3 to 22.5 μm, and cell wall thickness of about 1.45, 1.72, and 2.21 μm, respectively. Fig. 9(f) shows the microstructure of Mahogany contains hollow channels of various diameters that originate from tracheid cells that are parallel to the axis of the tree. The hollow channels of the biocarbon template have a uniform arrangement, where the black part is lumen, and the grey part is a carbon layer that is formed by carbonization of the cell wall. The difference in diameters of hollow channels is attributed to the non-uniform distribution of the texture of the wood. The average range of diameters of cell is about 5 ~ 30 μm, and the cell wall is about 2 ~ 3 μm thick. Most of the cellular pores show a rectangular shape, and the distribution shows a regular net with carbon wall joined to each other, as shown in Figs. 9(c) to (e). The topologically uniform arrangement of cell of early wood is interrupted by growing ring patterns, where late wood cell show a significantly higher strut thickness [107].

Physical properties of biomorphic carbon materials

Table 2 shows the physical properties of BCM with its unique structure obtained by pyrolysis of wood varieties, such as Cypress, Red pine, Gorman spruce, and Hard maple, respectively [108]. Carbonaceous materials impregnate and react with coated oxides and nano-oxides that can be used in a variety of applications, as well as filtration and catalyst support. Greil's research team [109, 110] was one of the first to report the characteristics of melt-impregnated bio SiC/Si, the properties of carbon preforms, and the mechanical properties of porous bioSiC obtained by gas infiltration

Table 2. Physical Properties of Biomorphic Carbon Materials.

Name	Compressive strength [MPa]	Pore size [μm]	Wall thickness [μm]	Pore morphology
Hard Maple	75.72	6.23	1.76	Circular
North American Ash	65.59	10.93	2.10	Circular
Cypress (Hinoki)	52.65	19.60	2.30	Hexagonal
North American Red Pine	44.70	34.33	1.45	Square
Red Pine	36.78	26.10	1.72	Square
Mahogany	31.74	8.91	2.49	Circular
Gorman Spruce	29.19	21.20	2.21	Square
Red Cedar	23.76	25.00	1.40	Hexagonal + Pentagonal

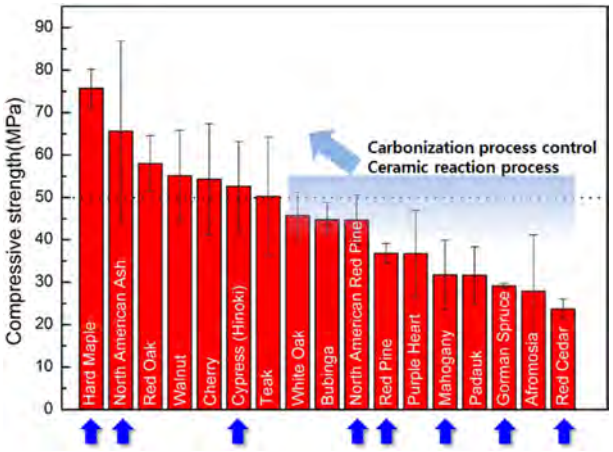

Fig. 10. Compressive strength of biomaterials after the carbonization.

[111-113]. Gutierrez-Mora et al. [114] and Presas et al. [115] studied the bending strength and fracture toughness of various bioSiC/Si materials derived from hardwood, using indentations to measure the hardness of eucalyptus, beech, and pine-derived bioSiC/Si composites [116, 117]. Park et al. [118] studied flexion and compressive strength as a function of the precursor density of bioSiC/Si synthesized by various precursors. Hou et al. [119] measured the bending strength as a function of penetration time to study the possible effects on the final properties of the material. Kaul et al. [120] measured the mechanical properties such as elastic modulus, compressive strength, and fracture toughness of the porous bioSiC from other precursors. Table 1 shows that the compressive strengths of Hinoki and Red cedar with pore size of 19.60, 25.0 μm, and wall thickness of 2.3 and 1.73 μm are 52.65 and 23.76 MPa, respectively.

In addition, the Red pine having a pentagonal and hexagonal honeycomb structure has a pore size of 36.78 μm, a wall thickness of 1.72 μm, and a compressive strength of 23.76 mpa. Fig 10 shows that the carbonized carbon materials reveal increased compressive strength due to the ceramic reaction.

Fabrication of CNTs composites

In principle, finely dispersed, nanometer-sized metal particle catalysts that preserve their morphology at the CVD processing temperatures are required, because controlling the morphology of the catalytic particles during CNTs growth strongly affects nanotube characteristics, such as thickness, uniformity, and yield. However, as the size of the metal particles decreases to the nanometer scale, they tend to agglomerate. To prevent this, porous materials have been proposed as supports. A porous support showing a non-continuous surface and high SSA can not only contribute expressively to particle stabilization and produce a fine dispersion of well-defined particles, but also radically increase the number of catalytic particles, thus increasing the number of nucleation sites, which are all advantageous to the synthesis of CNTs [121]. Commonly used substrates in CVD include silicon [122], quartz [123], silica [124], silicon carbide [125], alumina [126], alumino-silicate (namely, zeolite) [127, 128], and magnesium oxide [129]. Among all the catalytic supports, zeolites being molecular sieve materials with pore diameters in the range 3 ~ 10 Å have had a significant impact due to their structural homogeneity, and high reactive surface area, which makes them excellent host candidates for different types of adsorbing molecules [130]; and hence zeolites could be used as supports for catalyst particles to synthesize and grow CNTs [131]. In this review, the zeolite (LTA, Silicalite-1) and meso-porous SiO_2 are used as the templates for supporting catalyst nanoparticles to synthesize CNTs biomorphic carbon composites via the CCVD method.

Template-coated biomorphic carbon materials

Zeolites are typically defined as crystalline aluminosilicate with the chemical composition $M_x[(AlO_2)_x(SiO_2)_y]\cdot nH_2O$. Their structure is based on a three-dimensional regular connection of $[AlO_4]^{5-}$ and $[SiO_4]^{4-}$ tetrahedral units, which are linked to each other via bridging oxygen atoms. As each aluminum atom in the framework generates negative charge, cations (M^+) must exit for charge balancing in the framework [132]. The framework structures create unique three-directional features, high regular arrays of very open void spaces that are often termed cages or channels. Typically, the window diameter of its pores ranges 3 to 8 Å, while the inner diameter of interior spaces ranges 5 to 13 Å. Up to now, 235 types of zeolite frameworks are registered, having different 3-dimensional regular opened nanopore or nanochannel structures. Based on their structural features having high surface area, zeolites are commonly used as commercial adsorbents [133] and catalysts [134, 135]. Recently, this unique structural feature provides a vast templating system in applied synthesis fields, such as quantum dot [136-139], organic molecules [140, 141], etc. In particular, zeolites have also been extensively tested as template for carbon nanotubes, because their uniformly arranged nanopores and nanochannels can serve as nano templates for liberating series of three-dimensional ordered micro-porous carbon materials [142, 143]. We term this material 'zeolite-templated carbon' (ZTC). Generally, ZTCs of the three-dimensionally ordered framework by replicating the zeolite template are obtained only when the synthesis is carefully performed with appropriate conditions, which is comprised of three steps: (a) uniform carbon introduction only inside the zeolite nanochannels, (b) heat treatment, and (c) template removal [144, 145]. The first formation of porous carbon using zeolite templates was reported in 1997 with description of some of the unique advantages of this technology. By depositing

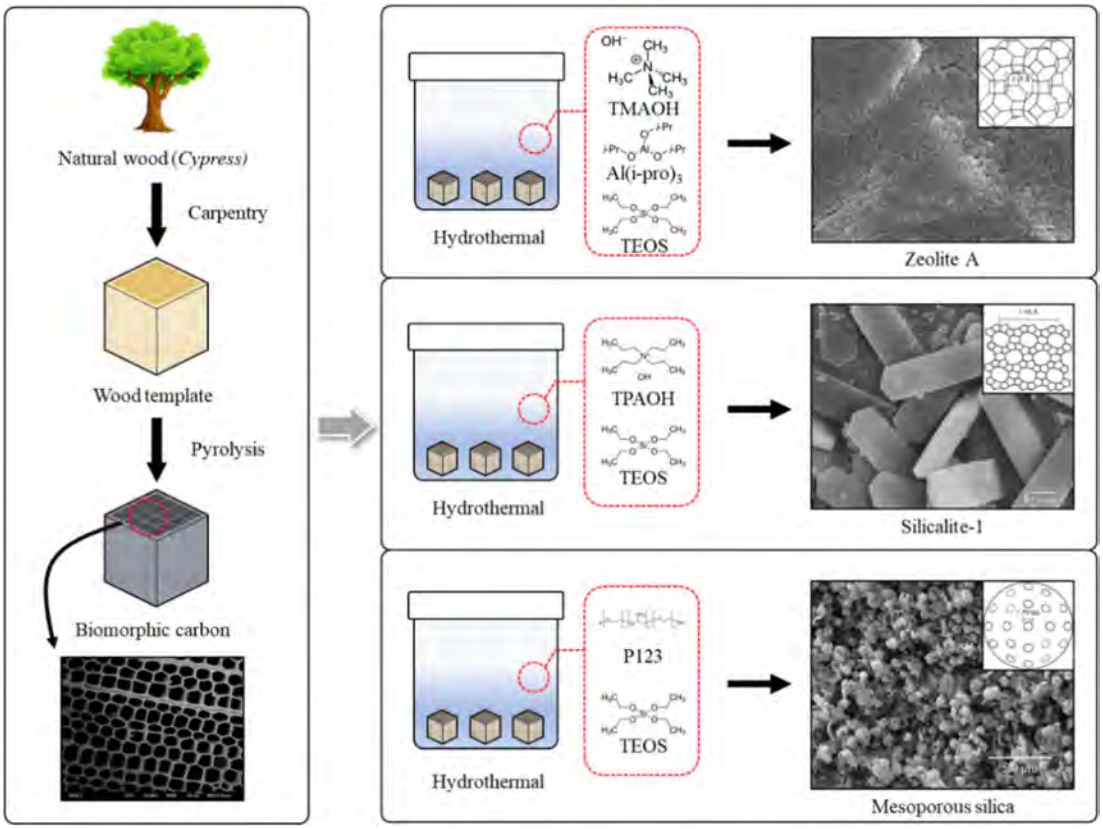

Fig. 11. Process for synthesizing and coating LTA, silicalite-1 and mesoporous silica onto BCMs (Modified from ref. 156. Copyright 2018 Hanyang University).

graphene monolayers uniformly on the internal surface area of zeolites, and by etching the zeolite using a combination of acids, porous carbon replicas may be produced with an ordered array of microspores. The large variety of zeolites with more than 200 types available allows an appropriate template to be selected for the desired pore size in a ZTC [146]. This review addresses surface modification of the mesoporous templates, such as Linde Type A (LTA) zeolite [147, 148], silicalite-1 [149-151], and mesoporous silica [152]. Among these matrices, zeolite is an excellent template for supporting or encapsulating catalyst nanoparticles due to the well-defined pore structure and high surface area and is responsible for catalyst particle stabilization and the fine dispersion of nanoparticles [153]. Generally, silicalite-1 is pure SiO_2 zeolite, and has high surface area. It also has the potential to load catalytic materials on the cavity of silicalite-1 of about 0.5 ~ 0.55 nm. But it is difficult to load some materials on its surface firmly or in its pores, due to its smooth surface and small cavity. In order to meet growing environmental challenges, it is important to explore new technologies to treat or synthesize silicalite-1, which can load a large amount of other materials, and retain its large surface area [154, 155]. The mesoporous structure features a large specific surface area and pore size of 2 to 50 nm in diameter. Mesoporous silica nanoparticles (MSNs) can also be used as a host material to carry therapeutic agent or for molecule encapsulation and can be used as a template for the synthesis of CNTs. Good biocompatibility, high loading capacity, and the possibility of attachment of a target ligand for specific cell recognition, or a well-defined and adjustable porosity design, make MSN suitable for drug delivery. Fig. 11 shows a new process for synthesizing and coating LTA zeolite, silicalite-1, and mesoporous silica onto biomorphic carbon materials [156].

Fig. 12 shows microstructures of (a) and (a') LTA type zeolite, (b) and (b') silicalite-1, and (c) and (c') mesoporous silica template coated cypress BCM. The LTA zeolites are finely coated inside and outside of the honeycomb structure, which can be observed in Fig. 12 (a'). The cubic shape of LTA zeolite crystals has been achieved with the size of around 120 nm in a configuration with a fine layer of well-controlled cube crystals. The cube {001} is composed of six perfect square faces that make angles of approximately 90 °. The crystal structure of LTA zeolites was homogeneously synthesized and coated on the surface of the template by an *in-situ* hydrothermal process. Generally, the framework of LTA zeolite crystals can be explained in terms of two types of polyhedra; one is a simple cubic alignment of eight tetrahedra, and is termed D4R, while the other is a truncated octahedron of 24 tetrahedra

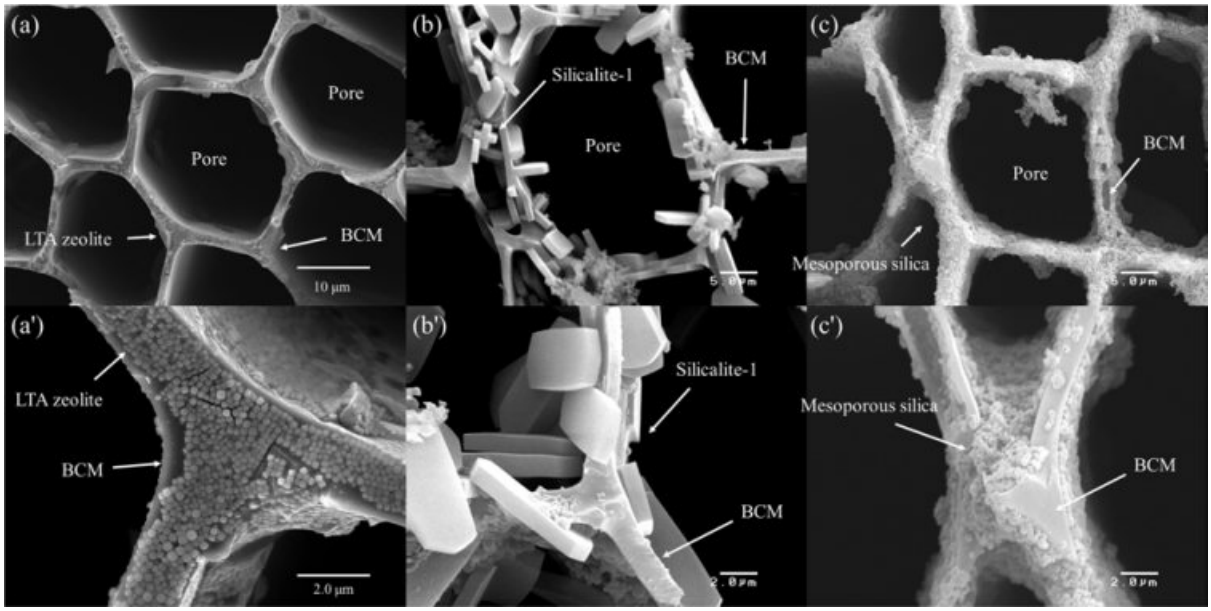

Fig. 12. FESEM images of cypress BCM coated with LTA (a), silicalite-1 (b), and mesoporous SiO_2 (c) (Modified from ref. 156. Copyright 2018 Hanyang University).

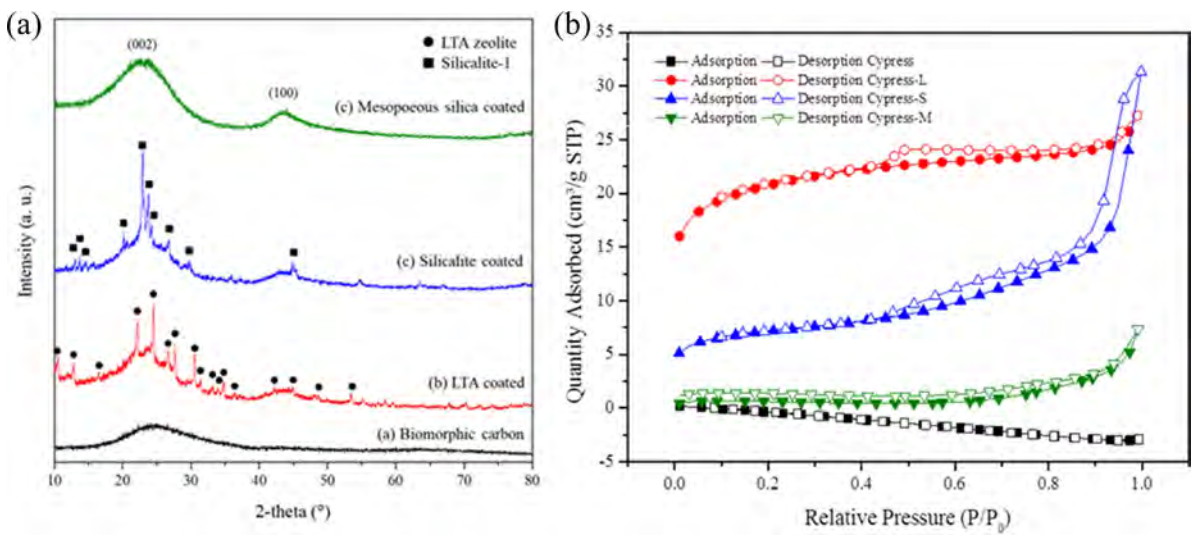

Fig. 13. XRD patterns (a) and N_2-adsorption/desorption isotherms (b) of BCM coated with LTA, silicalite-1, and mesoporous silica [156] (Modified from ref. 156. Copyright 2018 Hanyang University).

or cages, as previously described for the sodalite-type minerals [157, 158]. As observed with higher magnification, the 5.0 μm silicalite-1 particles were entirely interlocked and coated on the surface of BCM. The images revealed the presence of a continuous and smooth mesoporous silica film layer of less than 1.0 μm [156].

Fig. 13(a) shows XRD patterns of LTA, silicalite-1, and mesoporous silica template synthesized on the surface of the BCM. These XRD plots show different peaks, which indicate monolayer and multi-layer fine coating of the template. These peaks were then compared to JCPDS files. Compared to JCPDS file # 97-002-4901, the corresponding peaks reflected the yield of LTA phase, 2θ = 10 ° (220), and 24 ° (600). A single phase with an average lattice constant of 24.61 Å was found in the obtained XRD. This is a simple cubic arrangement of eight tetrahedra with D4R [21, 156]. Similarly, when the obtained XRD plots were compared to the JCPDS 42-0023 original JCPDS file for silicalite-1, corresponding peaks were also found. This assures the synthesis of silicalite-1 in the BCM. Randomly oriented silicalite-1 crystals were coated as shown in Fig. 12(b). BCM was also coated with mesoporous silica. However, it was hard to recognize it with wide angle XRD, due to the mesoporous silica's properties. Instead, it needed to be analyzed with small angle XRD [22, 156]. The peak intensity was the background of

amorphous carbon.

Fig. 13(b) shows the N_2-adsorption/desorption isotherms of BCM coated with LTA, silicalite-1, and mesoporous silica. According to the International Union of Pure and Applied Chemistry (IUPAC) classification, isotherms of all the samples studied belonged to type IV [23, 160], suggesting that these adsorbents are mesoporous materials. Capillary condensation phenomenon may occur in their pore channels. Fig. 13(b) shows that the N_2-adsorption capacity of silicalite-1 seems to be greater than that of LTA zeolite or mesoporous silica. This is probably because the pores of LTA zeolite and mesoporous silica are partially covered by the active ingredient [161, 162], thus reducing the surface area. Furthermore, the hysteresis loop shifts in the relative pressure range of 0.4 ~ 1.0. The BET isotherms graphs (Fig. 13) show a typical type (IV) with type II-like hysteresis loops, indicating the presence of mesopores in all samples (LTA zeolite, silicalite-1, mesoporous silica). The position of the inflection point of P/P_0 is related to the diameter of the mesoporous range. The sharpness of the step shows uniform mesoporous size distribution. Table 3 summarizes the results of BET and the yield. Templates were coated on BCM to increase the specific surface area, especially of silicalite-1. The BET surface areas of the original carbonized cypress, LTA zeolite, silicalite-1, and mesoporous silica were 2.126, 65.977, 99.634, and 1.496 m^2/g, respectively [156].

Fabrication of CNTs nanofilter composites

Fig. 14 shows that catalytic decomposition of acetylene (C_2H_2) on the BCM was carried out in a quartz boat centered in a horizontal tube furnace. The synthesis was carried out with application of the three different processing routes for CNTs composites. First of all,

Table 3. BET surface and yield of template coated cypress BCM.

Sample	Pore size of template [nm]	Mean crystal size [μm]	BET surface area [m^2/g]	Yield of template [%]
Cypress	-	-	2.127	-
Cypress-L	3.456	0.247	65.978	16.350
Cypress-S	11.095	7.524	99.635	25.940
Cypress-M	10.953	0.381	1.496	4.394

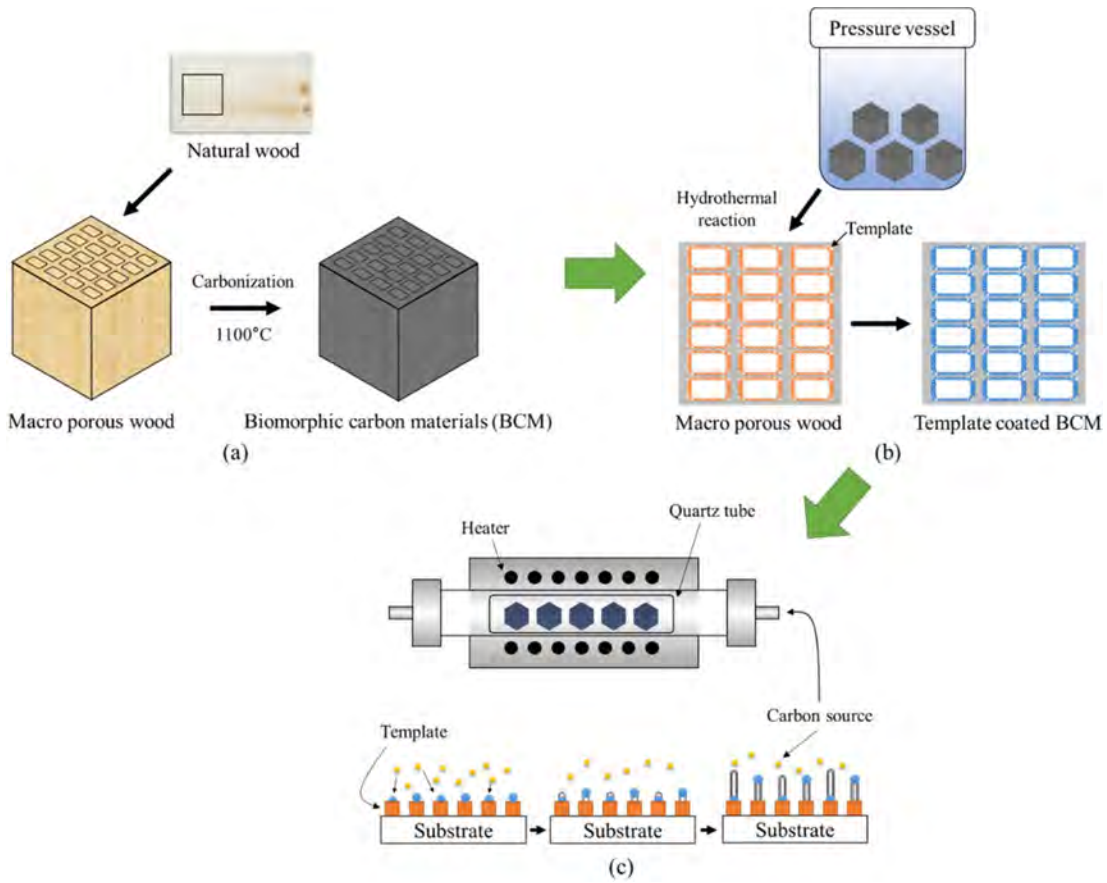

Fig. 14. Schematic diagram of growing Carbon nanotubes on BCM: Preparation of BCM (a), Template coating (b), and Carbon nanotube synthesis (c), respectively (Reproduced with permission from ref. 106. Copyright 2018 Inderscience Enterprises).

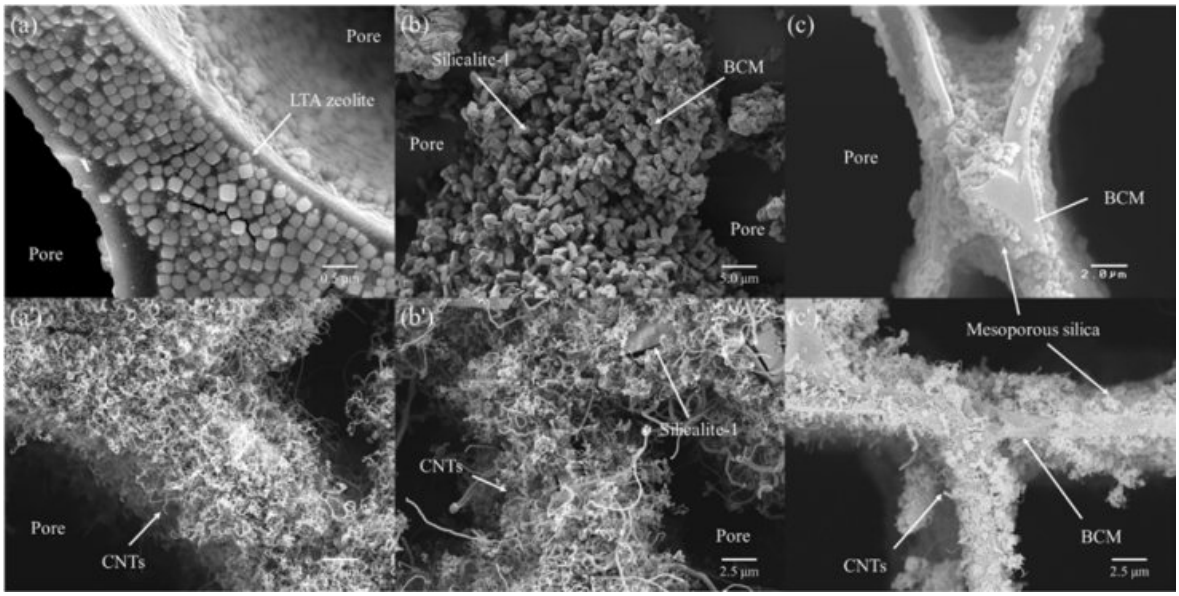

Fig. 15. FESEM image of Co- catalyst loaded template coated BCM and synthesized CNTs (') on (a) LTA zeolite, (b) Silicalite-1, and (c) Mesoporous SiO_2 template for 60 min at 650 ºC.

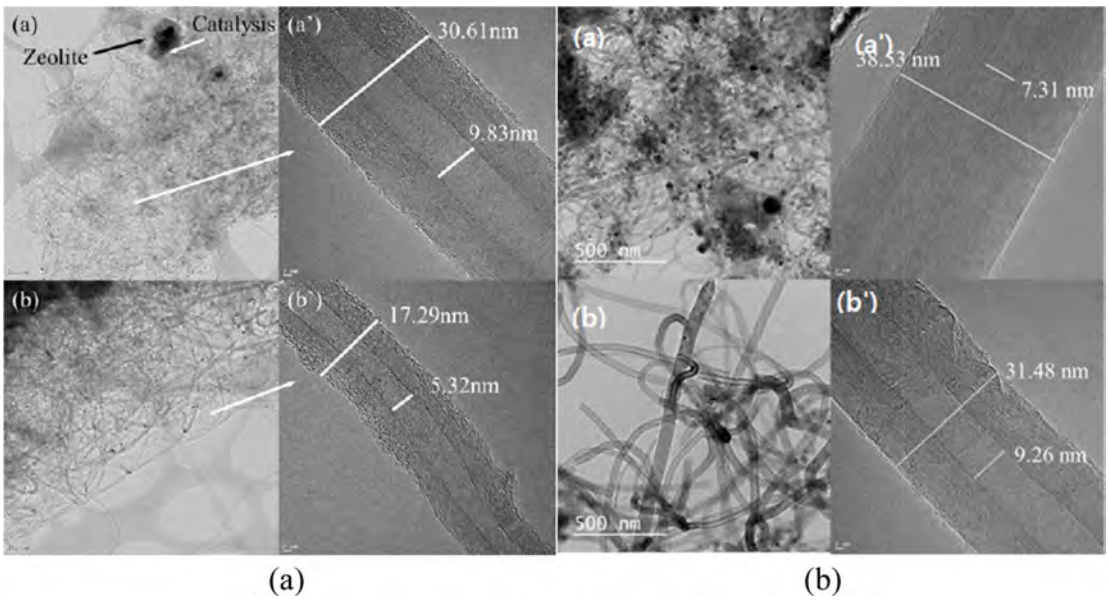

Fig. 16. HRTEM image of CNTs synthesis on Co-LTA(a) and Co-silicalite-1(b) coated BCM at 650 °C for (a) 60 min and (b) 120 min (Reproduced with permission from ref. 106. Copyright 2018 Inderscience Enterprises).

biomorphic carbon material was produced by the carbonizing reaction. Secondly, LTA [148] and silicalite-1 [151] were synthesized within and coated concurrently on the carbon template, which was then subjected to colloidal process, resulting in the formation of Co ions loaded on template-coated BCM substrate; and finally, the CCVD method was used for the synthesis of CNTs, as shown in Fig. 14(c) [163, 164]. To maintain neutrality, the temperature was elevated at a rate of 5 °C/min to the desired reaction temperature in a nitrogen atmosphere (200 sccm). Carbon nanotubes were grown by the introduction of carbon feeding gas C_2H_2@ 10 sccm. CNTs were separately synthesized at 650 and 700 °C for 40, 60, 120, and 180 min, respectively.

Fig. 15 shows FE-SEM images of multi-walled CNTs grown on Co- catalyst loaded LTA-, silicalite-1, and mesoporous SiO_2-BCMs for 60 min at 650 °C, respectively. Figs. 15(a), (b), and (c) clearly show the CNTs synthesized on the BCM keeping template as a base for the FESEM images in overview, respectively. All templates were uniformly and tightly coated on the BCM surface. All CNTs were synthesized as multi-layered carbon nanotubes like hair, so the yield of CNTs was very low in mesoporous SiO_2 template, as shown in Fig. 16.

Fig. 16(a) shows the HRTEM images of multiwall

CNTs (MWCNTs) that were grown on (a) and (a,) Co-LTA-BCM and (b) and (b,) Co-silicalite-1-BCM at 650 °C for 60 and 120 min, respectively. The CNTs in the TEM image of Fig. 16(a) show small outer walls with a diameter of approximately 17.29 nm and an inner diameter of 5.32 nm. The outer walls of the synthesized CNTs in Fig. 16(b) are comparatively thicker, and a densely layered structure with outer and inner diameters of approximately 30.61 and 9.83 nm, respectively, was formed. A base growth mechanism can be clearly seen in the CNTs, which are known for better attachment tendencies regarding the substrate. Also, note here the apparent growth of the inner and outer diameters of the nanotubes. Thus, it can be inferred that the decomposition of the carbon atoms from C_2H_2, which formed a layered coaxial cylindrical graphene sheet around the CNT core, is strongly related to the reaction time and temperature. All of the CNT samples display a bamboo-like structure and are typically MWCNTs. Moreover, it can be clearly inferred from the following HRTEM images that the CNTs that were grown at 650 °C produced a superior yield with smoother outer and inner walls, compared to the ones synthesized at 700 °C [164, 165].

Figs. 16(b) and (b') show the HRTEM images of multi-walled CNTs grown on Co-silicalite-1-BCM at 650 °C for (a) 60 min, and (b) 120 min, respectively. Fig. 16(b) shows thicker outer walls, with a diameter of around 31.48 nm. with an inner diameter of 9.26 nm Also, note here the apparent growth in terms of the inner and outer diameters. The synthesized CNTs at the same temperature for 120 min shown in Fig. 16(b') have a comparatively thicker outer wall, which forms a densely layered structure with an outer diameter of around 38.53 nm and inner diameter of 7.31 nm. Moreover, it can clearly be inferred from the HRTEM images below that the CNTs grown for 120 min have better yield with smooth outer and inner walls, in comparison to the one synthesized for 60 min [166].

Fig. 17 shows the TGA curves of the CNTs grown on Co-LTA BCM at 650 °C for (a) without CNTs, (b) 40 min, (c) 60 min, (d) 120 min, and (e) 180 min, respectively. All samples represent an initial weight loss tendency, which may occur through the loss of physically adsorbed water by the zeolites until 195 °C. In the continuous increment of reaction time, all samples undergo a weight loss pattern [165]. As compared with Fig. 17 (a), all CNTs samples show a weight loss i.e. (b) 2.8 %, (c) 5.61 %, (d) 6.95 %, and (e) 7.03 %, respectively. These differences of weight loss can be explained by carbon yield. The carbon yield from CNTs synthesized by metal containing CVD is calculated as follows:

$$\text{Carbon yield (\%)} = (m_{tot} - m_{cat})/m_{cat} \times 100\% \quad (1)$$

where, m_{cat} is the initial catalyst amount (before reaction), and m_{tot} is the total sample weight after synthesis [166]. The TGA curves allow estimation of the amount of carbon yield.

Fig. 17(b) shows the Raman spectra of the synthesized CNTs. In these results, two strong peaks can be observed within the wavelengths 1,340 and 1,600 cm^{-1}, designated as D- and G-bands, respectively. These represent the presence of defects in the graphitic sheets, and crystalline graphite carbon [166, 167]. The strength of the D-band relative to the G-band is a measure of the amount of disorder in the CNTs and is used for the qualitative analysis of nanotubes. The relative intensities of the D- to G- bands (the I_D/I_G ratio) revealed by the Raman spectroscopy is a measure of the degree of graphitization. The I_D/I_G values are between 0.59 and 1.00, which is in accordance with those reported in the literature (I_D/I_G = 0.7 ~ 1.3) for CVD grown MWCNTs [168, 169], revealing the high-quality MWCNTs was grown.

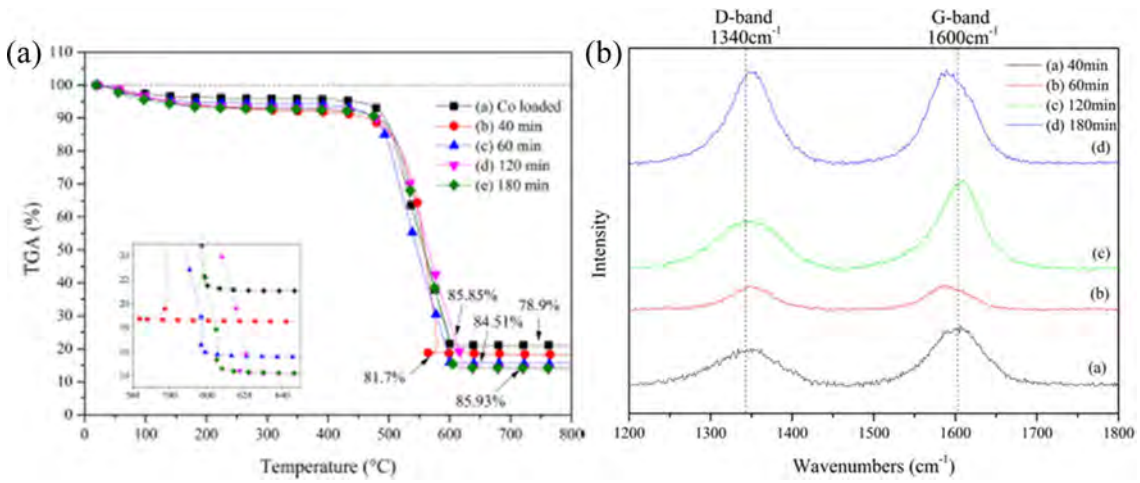

Fig. 17. TGA curves (a) and Raman spectra (b) of CNTs synthesized on Co-LTA Gorman spruce BCM (Adapted from ref. 166. Copyright 2017 Hanyang University).

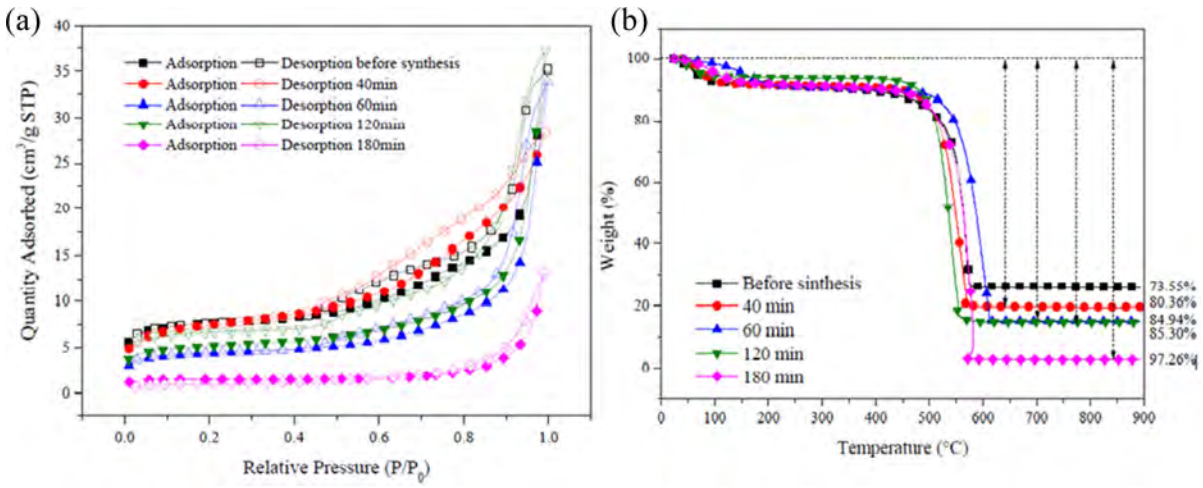

Fig. 18. TGA curves(a) and BET surface area(b) of CNTs synthesis on silicalite-1 coated biomorphic carbon (Adapted from ref. 178. Copyright 2019 Hanyang University).

Fig. 18(a) shows the N_2 adsorption/desorption isotherms of Co-silicalite-1 BCM and CNTs grown at 650 °C for 40, 60, 120, and 180 min, respectively. The adsorption and desorption isotherms of N_2 for the Co loaded silicalite-1 on BCM and CNTs grown at 650 °C for (b) 40 min, (c) 60 min, (d) 120 min, and (e) 180 min are clearly of type IV, according to the IUPAC classification of adsorption isotherms. Type IV isotherms characteristically show the simultaneous presence of micro- and mesopores. It is evident that the adsorption capacities of CNTs were all increased with the increase in reaction time [170-172]. All of the samples demonstrate relatively high adsorption performance. Compared with Co-silicalited-1-BCM, the adsorption capacity of CNTs silicalite-1 supported BCM is markedly lower. For CNTs Co- silicalite-1-BCM, silicalite-1-BCM is the skeleton and is coated on it, and then the silicalite-1 supported biomorphic carbon would be the main adsorbent, as shown in Fig. 12(b).

Fig. 18(b) shows the TGA curves of the CNTs grown for 40, 60, 120, and 180 min at 650 °C, respectively. All CNTs samples represent an initial weight loss tendency, which may occur through the loss of physically adsorbed water by the silicalite-1 until 195 °C. In the subsequent heating process, all samples undergo a two-step weight loss pattern up to 97%. In the first step (458 ~ 633 °C and 485 ~ 717 °C, respectively), the amorphous carbon has been combusted, while in the second step (≥ 633 and 717 °C, respectively), the MWCNTs have combusted until 800 °C.

After that, the samples maintain a weight loss pattern due to biomorphic carbon combustion. The main reason for the two-step pattern is that the decomposition of C_2H_2 on metal catalysts leads to the formation of CNTs as amorphous carbon [173, 174].

All Raman spectra are dominated by two strong peaks at 1,340 and 1,620 cm^{-1}. The accepted terms for these two peaks are the D- and G-bands, respectively. They are characteristic for disordered sp^2-hybridised carbon materials and have been observed in all reported Raman spectra of MWCNTs. The D-band is formed by the defects in the graphite crystals, and by the finite sizes of graphite crystallites in the material. Moreover, pyrolytic carbon particles deposited on the nanotubes also contribute to the rise of D-band. The G-band corresponds to the tangential stretching (E_{2g}) mode of highly oriented pyrolytic graphite (HOPG) and indicates the presence of crystalline graphitic carbons in the MWCNTs. The strength of the D-band relative to the G-band is a measure of the amount of disorder in the CNTs and is used for qualitative characterizations of the nanotubes [175, 176]. Table 3 shows the relative intensities of the D- to G- bands (I_D/I_G ratio), as revealed by Raman spectroscopy, which is a measure of the degree of graphitization. The carbon yield of 6.81 to 23.71% followed by BET ranging 4.31 to 22.24 m^2/g was achieved with the reaction time of 40 to 180 min, followed by the I_D/I_G values from this work, which are between 0.99 and 1.01, which is in accordance with that reported in the literature (I_D/I_G = 0.97 ~ 1.00) for CVD-grown MWNTs [177, 178].

This finding can be attributed to the low permeability

Table 4. Quality of CNTs (Raman spectra) and Carbon Yield (TGA) with respect to the Reaction Time at 650 °C.

Sample	Carbon yield [%]	Raman ratio [I_D/I_G]
CoLTA-G. Spruce - 40 min	2.80	1.00
CoLTA-G. Spruce - 60 min	5.61	0.81
CoLTA-G. Spruce - 120 min	6.95	0.98
CoLTA-G. Spruce - 180 min	7.03	0.59
CoSilicalite-Cypress - 40 min	6.81	1.01
CoSilicalite-Cypress - 60 min	11.39	1.00
CoSilicalite-Cypress - 120 min	11.75	0.99
CoSilicalite-Cypress - 180 min	23.71	0.99

of 1.99×10^{-8} m^2 compared to that of cypress (Hinoki, 1.51×10^{-6} m^2), which was tested using Darcy's law [179]. Table 4 summarizes the physical properties of the Co-LTA and silicalite-1-BCM and CNTs grown at 650 °C for 40, 60, 120, and 180 min, such as carbon yield and Raman ratio.

CNTs Nanofilter Applications

Air and water pollution in industrial and metropolitan areas is a threat to human health and natural resources, as millions of people inhale polluted air, and particles in the air enter the body. Fine particles can be trapped in the nostrils and can be in the hair at nano size below a micron, but some fine particles can reach the lungs, and then remain in the lung cells, causing serious diseases, such as lung cancer or emphysema [180]. Clean air and water (no toxic chemicals and pathogens) play a very important role in the human quality of life [181]. Water and air are important sources of various food industries for maintaining good health, including medicines [182]. In particular, it is difficult to remove organisms such as bacteria and viruses from food, and much research is being carried out on the contamination of inorganic substances (e.g. heavy metal ions) from water, especially in the wastewater, metallurgy, mining, and battery manufacturing industries [183]. Since these contaminants can accumulate in living tissues, there is an increasing concern, and more stringent regulations and standards for the discharge and removal of aquatic environments are being discussed. At present, innovations and advances in nanotechnology and nanomaterials can solve many of the above-mentioned problems, in particular carbonaceous nanomaterial complexes. Individual and bulk carbon-based nanomaterials have already paved the way for many environmental applications. In particular, CNTs exhibit large absorption properties, due to their high aspect ratio, and large specific surface area. They offer promise for applications in the absorption, filtration, and separation industries, in both gas and aqueous systems [180, 184].

- Air particulate filtration [185, 186]
- Biological contamination filtration [190, 191]
- Heavy metal ion adsorption [192, 193]
- Other applications [197, 198]

Air particulate filtration

Heating, ventilation, and air conditioning (HVAC) filters are ideal for dark, humid air cleaning. As conditions for bacteria and malignant fungus, microorganisms become attached to the accumulated dust in the filter, polluting the unpredictable air quality, as well as accumulating the smell of dust in food. Nanofiber filter media are needed for high-performance air purification, such as hospitals, medical facilities, and laboratories [180]. In air filtration, especially in laboratories, electronic component manufacturers, military and government agencies, and food, pharmaceutical, and biotechnology companies, contaminants are particles and mostly complex mixtures, which are generally less than 1,000 μm in diameter [185]. Fiber filters are typically fabricated from fibers with a diameter of about a few tens of micrometers, which is a micrometer particle that enables high efficiency removal of the sub-micrometer and has a relatively low resistance to air flow. The filter is termed the most penetrating particle size (MPPS), which is not as efficiently filtered as other particles, and the fiber filter efficiency achieves the minimum value for this particle size, which is generally between 0.1 and 0.5 μm [186, 187]. Park and Lee [188] grew CNTs 20 ~ 50 nm diameter using the CVD method on micron-sized stainless steel fibers and evaluated the performance of air particulate removal using sodium chloride (NaCl) as test particles, as shown in Fig. 19. Web-like CNTs were fabricated to improve the efficiency from 75 to 98%. Park's group reported similar results using fiberglass [189].

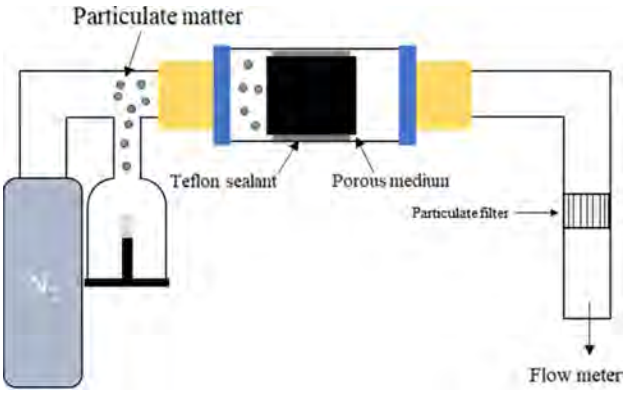

Fig. 19. Schematic diagram of air filter evaluation of CNTs nanofilter.

Biological contamination filtration

Biological contaminants make up a significant portion of drinking water, in terms of the number of pollutants and the treatment probability. High-efficiency filtration of contaminants is performed using ceramic or metal membranes [180, 190]. The polymer membrane is fragile and durable. In conventional membrane filters used for water filtration, the adsorption of bacteria on the surface affects the physical properties and is difficult to reuse. The use of CNTs in membranes is also an effective way to create a practical hybrid filter with excellent robustness for reuse. With high surface area and large aspect ratio, high-density coagulated packed CNTs form a microporous and mesoporous network with an appropriate pore size, which adsorbs contaminants through physisorption [191, 192]. In addition, the toxicity of microbial cells also plays a part in the filtration performance of CNTs. The stability of CNTs at high temperatures enables higher operating temperatures up to 400 °C. Compared with conventional polymer

membrane filters up to 52 °C, these filters are very good, and for their reuse, simple filter cleaning is sufficient for ultrasonication and autoclaving sterilization up to 121 °C for 30 minutes. Brady-Estevez et al. increased filter permeability by immobilizing CNTs deposited on microporous ceramic filters with 5 μm pore size. They demonstrated a filter to remove viral and bacterial pathogens with very high efficiency [193]. Akasaka and Watari have shown that moderately flexible SWCNTs and MWCNTs can be easily wound around the curved surface of Streptococcus mutans, and used as a tool to remove nano-level oral pathogens, as shown in Fig. 20 [194]. First, the CNTs was dispersed in a solution containing bio-contaminants, the suspension was shaken for a long time to achieve complete adsorption, and then the CNTs was removed using a paper filter or a suitable membrane.

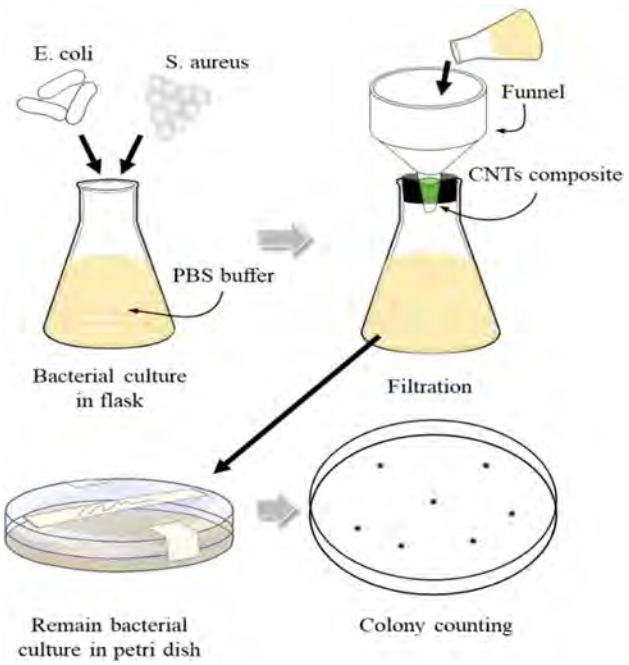

Fig. 20. Schematic of biological contamination filtration of CNTs nanofilter.

Heavy metal ion adsorption

Water pollution caused by indiscriminate disposal of metal ions has attracted worldwide attention [197]. In this regard, a number of studies have attempted to use CNTs to remove such contaminants from wastewater. Contaminants include Cu, Pb, Cd [195], Zn, Mn, Co [196], Ni [297], Cr [198], Hg [199], and U [200] ions. Figure 21 shows that the adsorption mechanism of heavy metals by CNTs is a chemisorption process. The chemical interaction between metal ions and metal ions is dominated by the surface functionalities of CNTs formed during oxidation rather than physical adsorption, which is compared to electrostatic attraction and adsorption-precipitation [201]. As a result, the chemical and thermal treatments during the functionalization process have a leading influence on the performance of CNTs for metal ion removal, and the adsorption behavior is mainly determined by the nature and concentration of the adsorbent surface functional group. Other terms and aspects of heavy metal ion adsorption through CNTs synthesized and functionalized with different adsorption capacities and different carbon sources and catalysts include effective parameters. For example, increasing adsorption temperatures result in a significant increase in adsorption capacity [202, 203]. This is an endothermic reaction. As the mass of CNTs increases, the adsorption rate of the metal increases. This is limited to a certain value with an increase in the number of adsorption sites.

Other applications

There are many other reports that have shown the

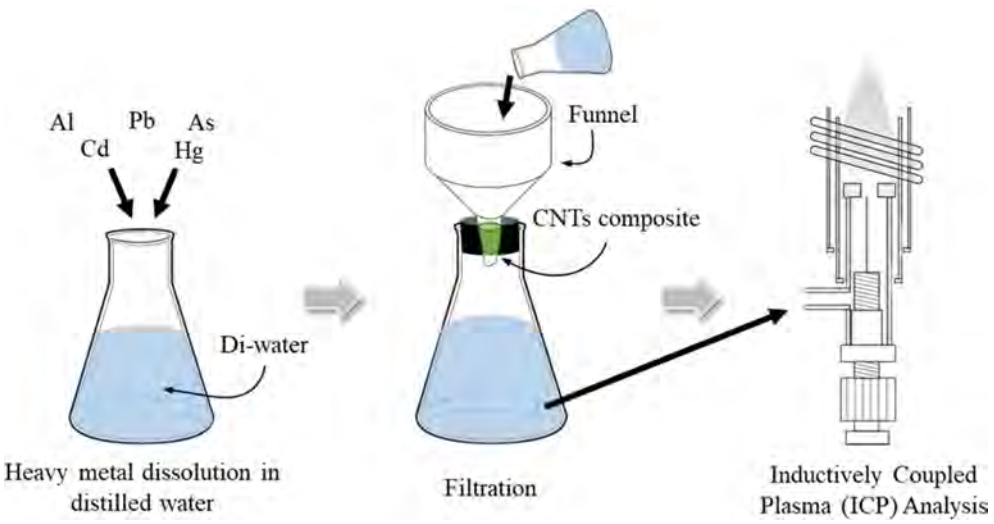

Fig. 21. Schematic of the heavy-metal adsorption of CNTs nanofilter.

successful use of CNTs in filtering applications [180]. Sponges have been successfully synthesized with CNTs by Gui et al., and could clearly reflect the large adsorption properties of these carbon clusters [204]. They produced self-assembled and interconnected carbon nanotube backbone sponge-like bulk materials close to airgels with > 99 % porosity and light density. Lee and Baik also produced nanotube membrane filters that can affect the phase separation of diesel and aqueous layers, surfactant stabilized emulsions, high viscosity lubricants, and water emulsions [205]. They deposited a mesh-on-mesh using an electron beam evaporator and made a filter on a stainless-steel mesh using a sandwich type iron catalyst layer, followed by a CVD process. Mainstream smoke (MS), published by Chen et al., has a very high adsorption capacity of oxidized CNTs (O-CNTs) to nicotine and tar, and adds about (20 ~ 30) mg to the filter tip of tobacco, to prevent the influx of harmful substances [206].

Conclusions and Future Perspective

The unique properties of CNTs, including high surface area and strong Van der Waals forces at high aspect ratios, make them exceptional in their ability to filter organic and inorganic contaminants on a molecular basis. In particular, they exhibit a variety of processing capacities to trap and fix contaminants in the pores of individual CNTs during flocculation, and also to trap large-scale pore-sized mesoporous networks with biological contaminants, such as bacteria and viruses. A wide range of pore formation through the combination of CNTs and porous ceramics can be advantageously used as a filter for gas through physisorption. In particular, since the cytotoxicity of CNTs in microbial treatment partially affects the filtration performance, an approach that can be effectively applied in water as well as atmospheric filtration devices has been studied. In this review, carbon nanotubes (CNTs) synthesized on metal-supported template (LTA, silicalite-1, mesoporous SiO_2 etc.) coated biomorphic carbon materials (BCM) were achieved with both high quality, and high yield of carbons. The amounts of MWCNTs were formed by the combination of three different novel processing routes. Because of the uniform pore structure, the template crystals can be located all over the BCM surface. Also, owing to the high porosity template crystals, the acetylene can supply carbon source to the catalytic metal nanoparticles appropriately, to lead the growth of CNTs across the entire template. The morphology of CNTs was influenced by reaction temperature. The microstructure obtained at 700 °C exhibited considerable wall thickness, and the widest inner hollow tube structure; whereas that of CNTs obtained at 650 °C shows comparability thinner outer wall and narrow inner hole. The maximum yield of carbon was 23.71% at 650 °C for 180 min, but on comparison with the Raman ratio, the synthesized CNTs were found to have better quality at (60 to 120) min, with a moderate yield of carbon. The I_D/I_G ratio of Co-silicalite-1-BCM from Raman analysis was found between 0.97 and 1.00, which is in accordance with those reported in the Co-LTA-BCM for CVD-grown MWNTs. Furthermore, the synthesized CNTs filter can be applied as a filter for removing various pollutants. Especially, the filters are expected to be used in HVAC, water quality and air purification through performance evaluation such as air particulate, biological contamination and heavy metal filtration.

Acknowledgments

This research was supported by the Basic Science Research Program through the National Research Foundation of Korea (NRF), funded by the Ministry of Education (201800790001) and special thanks for analysis support and biomorphic carbon materials from Korea Institute of Energy Research (KIER).

References

1. F.S. Rojas, C.B. Ojeda, and J.M.C. Pavón, Am. J. Anal. Chem. 2[1] (2011) 66-74.
2. A. Zampieri, H. Sieber, T. Selvam, G.T. Mabande, W. Schwieger, F. Scheffler, M. Scheffler, and P. Greil, Adv. Mater. 17[3] (2005) 344-349.
3. Y. Shen, J. Agric. Food. Chem. 65[5] (2017) 995-1004.
4. S.Y. Kim, H.U. Kim, Y.H. Seong, I.S. Han, S.K. Woo, and S.H. Kim, J. Porous Mater. 25[2] (2018) 603-609.
5. J.G. Park, S.Y. Kim, Z. Wei, J.H. Jeon, S.Y. Kim, and I.J. Kim, J. Ceram. Proc. Res. 18[2] (2017) 161-165.
6. J. Li, Q. Xu, J. Wang, J. Jiao, and Z. Zhang, Ind. Eng. Chem. Res. 47[20] (2008) 7680-7685.
7. K.B. Choi, J.Y. Kim, S.M. Lee, K.H. Lee, and D.H. Yoon, J. Korean Ceram. Soc. 54[3] (2017) 257-260.
8. W. Zhao, B. Basnet, and I.J. Kim, J. Adv. Ceram. 1[3] (2012) 179-193.
9. S. Iijima and T. Ichihashi, Nat. 363[6430] (1993) 603-605.
10. C. Yu, L. Shi, Z. Yao, D. Li, and A. Majumdar, Nano. Lett. 5[9] (2005) 1842-1846.
11. K. Lee, S.Y. Shin, and Y.S. Yoon, J. Korean Ceram. Soc. 53[3] (2016) 376-380.
12. Y.L. Kim, J. Korean Ceram. Soc. 54[1] (2017) 66-69.
13. J. K. Holt, H. G. Park, Y. Wang, M. Stadermann, A. B. Artyukhin, C. P. Grigoropoulos, A. Noy, and O. Bakajin, Science 312[5776] (2006) 1034-1037.
14. Y. Zhao, H. Nakano, H. Murakami, T. Sugai, H. Shinohara, and Y. Saito, Appl. Phys. A. 85[2] (2006) 103-107.
15. V.K.K. Upadhyayula, S. Deng, M.C. Mitchell, and G.B. Smith, Sci. Total. Environ. 408[1] (2009) 1-13.
16. A.S. Brady-Estévez, S. Kang, and M. Elimelech, Small 4[4] (2008) 481-484.
17. A. Stafiej and K. Pyrzynska, Sep. Purif. Technol. 58[1] (2007) 49-52.
18. Y.H. Li, J. Ding, Z. Luan, Z. Di, Y. Zhu, C. Xu, D. Wu, and B. Wei, Carbon 41[14] (2003) 2787-2792.
19. Y.H. Li, Y.M. Zhao, W.B. Hu, I. Ahmad, Y.Q. Zhu, X.J. Peng, and Z.K. Luan, J. Phys. Conf. Series. 61 (2007) 698-702.

20. A. Srivastava, O.N. Srivastava, S. Talapatra, R. Vajtai, and P.M. Ajayan, Nat. Mater. 3[9] (2004) 610-614.
21. N. Halonen, A. Rautio, A.R. Leino, T. Kyllonen, G. Toth, J. Lappalainen, K. Kordas, M. Huuhtanen, R.L. Keiski, A. Sapi, M. Szabo, A. Kukovecz, Z. Konya, I. Kiricsi, P.M. Ajayan, and R. Vajtai, ACS. Nano 4[4] (2010) 2003-2008.
22. P.M. Ajayan, Chem. Rev. 99[7] (1999) 1787-1800.
23. W.Z. Li, J.G. Wen, Y. Tu, and Z.F. Ren, Appl. Phys. 73[2] (2001) 259-264.
24. D.J. Kim, S.M. Jeong, S.G. Yoon, C.H. Woo, J.I. Kim, H.G. Lee, J.Y. Park, and W.J. Kim J. Korean Ceram. Soc. 53[6] (2016) 597-603.
25. C. Weilach, C. Spiel, K. Föttinger, and G. Rupprechter, Surf. Sci. 605[15] (2011) 1503-1509.
26. K. An, N. Musselwhite, G. Kennedy, V.V. Pushkarev, L.R. Baker, and G.A. Somorjai, J. Colloid Interface Sci. 392 (2013) 122-128.
27. Y.M. Kim and I.J. Kim, J. Korean Ceram. Soc. 43[1] (2006) 1-3.
28. S.J. Park and D.G. Lee, Curr. Appl. Phys. 6[S1] (2006) e182-e186.
29. W. Zhao, S.D. Nam, A. Pokhrel, J. Gong, and I.J. Kim, J. Korean Ceram. Soc. 50[1] (2013) 1-17.
30. I.J. Kim, W. Zhao, X. Fan, J.H. Chang, and L.J. Gauckler, J. Ceram. Proc. Res. 11[2] (2010) 158-163.
31. Y. Yang, Z. Hu, Y.N. Lü, and Y. Chen, Mater. Chem. Phys. 82[2] (2003) 440-443.
32. K.S. Novoselov, A.K. Geim, S.V. Morozov, D. Jiang, Y. Zhang, S.V. Dubonos, I.V. Grigorieva, and A.A. Firsov, Science 306[5696] (2004) 666-669.
33. S. lijima and T. Ichihashi, Nat. 364[6439] (1993) 737-737.
34. K.W. Kolasiniski, in "Surface Science: Foundations of Catalysis and Nanoscience" (Wiely, 2012) p. 18.
35. A.P. Graham, G.S. Duesberg, W. Hoenlein, F. Kreupl, M. Liebau, R. Martin, B. Rajasekharan, W. Pamler, R. Seidel, W. Steinhoegl, and E. Unger, Appl. Phys. A. 80[6] (2005) 1141-1151.
36. R. Saito, in "Physical Properties of Carbon Nanotubes" (World Scientific Publishing Company, 1998) p. 36.
37. G.D. Nessim, Nanoscale. 2[8] (2010) 1306-1323.
38. D. Dass, R. Prasher, and R. Vaid, Int. J. Comput. Eng. Res. 2[5] (2012) 1447-1457.
39. Z. Xu, X. Bai, Z. L. Wang, and E. Wang, J. Am. Chem. Soc. 128[4] (2006) 1052-1053.
40. H.W. Zhu, C.L. Xu, D.H. Wu, B.Q. Wei, R. Vajtai, and P.M. Ajayan, Science 296[5569] (2202) 884-886.
41. H. Kataura, Y. Kumazawa, Y. Maniwa, I. Umezu, S. Suzuki, Y. Ohtsuka, and Y. Achiba, Synth. Met. 103[1] (1999) 2555-2558.
42. B.I. Kharisov. O.V. Kharissova, and U. Ortiz-Mendez, in "Handbook of Less-Common Nanostructures" (CRC Press, 2012) p. 31.
43. P.G. Collins, A. Zettl, H. Bando, A. Thess, and R.E. Smalley, Science 278[5335] (1997) 100-102.
44. M. Nihei, A. Kawabata, D. Kondo, M. Horibe, S. Sato, and Y. Awano, Jpn. J. Appl. Phys. 44[4A] (2005) 1626-1628.
45. R.H. Baughman, C. Cui, A.A. Zakhidov, Z. Iqbal, J.N. Barisci, G.M. Spinks, G.G. Wallace, A. Mazzoldi, D.D. Rossi, A.G. Rinzler, O. Jaschinski, S. Roth, and M. Kertesz, Science 284[5418] (1999) 1340-1344.
46. C. Liu, Y.Y. Fan, M. Liu, H.T. Cong, H.M. Cheng, and M.S. Dresselhaus, Science 286[5442] (1999) 1127-1129.
47. C. Liu, Y. Tong, H.M. Cheng, D. Golberg, and Y. Bando, Appl. Phys. Lett. 86[22] (2005) 223114.
48. J. Kong, E. Yenilmez, T.W. Tombler, W. Kim, H. Dai, R.B. Laughlin, L. Liu, C.S. Jayanthi, and S.Y. Wu, Phys. Rev. Lett. 87[10] (2001) 106801.
49. C. Zhou, J. Kong, and H. Dai, Appl. Phys. Lett. 76[12] (2000) 1597-1599.
50. D. Yokoyama, T. Iwasaki, K. Ishimaru, S. Sato, T. Hyakushima, M. Nihei, Y. Awano, and H. Kawarada, Jpn. J. Appl. Phys. 47[4] (2008) 1985-1990.
51. A. Javey, J. Guo, Q. Wang, M. Lundstrom, and H. Dai, Nat. 424 (2003) 654-657.
52. P.G. Collins, M.S. Arnold, and P. Avouris, Science 292[5517] (2001) 706-709.
53. S. Frank, P. Poncharal, Z.L. Wang, and W.A. Heer, Science 280[5370] (1998) 1744-1746.
54. A. Naeemi and J.D. Meindl, IEEE Electron. Device. Lett. 27[5] (2006) 338-340.
55. H.J. Li, W.G. Lu, J.J. Li, X.D. Bai, and C.Z. Gu, Phys. Rev. Lett. 95[8] (2005) 086601.
56. J.P. Lu, Phys. Rev. Lett. 79[7] (1997) 1297-1300.
57. J.P. Salvetat, J.M. Bonard, N.H. Thomson, A.J. Kulik, L. Forró, W. Benoit, and L. Zuppiroli, Appl. Phys. A. 69[3] (1999) 255-260.
58. M.F. Yu, B.S. Files, S. Arepalli, and R.S. Ruoff, Phys. Rev. Lett. 84[24] (2000) 5552-5555.
59. N. Yao, and V. Lordi, J. Appl. Phys. 84[4] (1998) 1939-1943.
60. G. Zhou, W. Duan, and B. Gu, Chem. Phys. Lett. 333[5] (2001) 344-349.
61. Z. Yao, C.C. Zhu, M. Cheng, and J. Liu, Comput. Mater. Sci. 22[3] (2001) 180-184.
62. B.G. Demczyk, Y.M. Wang, J. Cumings, M. Hetman, W. Han, A. Zettl, and R.O. Ritchie, Mater. Sci. Eng. A. 334[1] (2002) 173-178.
63. J. Hone, M. Whitney, and A. Zettl, Synth. Met. 103[1] (1999) 2498-2499.
64. E. Pop, D. Mann, Q. Wang, K. Goodson, and H. Dai, Nano. Lett. 6[1] (2006) 96-100.
65. P. Kim, L. Shi, A. Majumdar, and P.L. McEuen, Phys. Rev. Lett. 87[21] (2001) 215502.
66. R.H. Fowler and L. Nordheim, Proc. R. Soc. London. Ser. A. 119[781] (1928) 173-181.
67. S. Fan, M.G. Chapline, N.R. Franklin, T.W. Tombler, A.M. Cassell, and H. Dai, Science 283[5401] (1999) 512-514.
68. H. Zhu, J. Wei, K. Wang, and D. Wu, Sol. Energy Mater. Sol. Cells 93[9] (2009) 1461-1470.
69. E. Kymakis, I. Alexandrou, and G.A.J. Amaratunga, J. Appl. Phys. 93[3] (2003) 1764-1768.
70. A. Kongkanand, R.M. Domínguez, and P.V. Kamat, Nano. Lett. 7[3] (2007) 676-680.
71. C. Journet, W.K. Maser, P. Bernier, A. Loiseau, M.L. de la Chapelle, S. Lefrant, P. Deniard, R. Lee, and J.E. Fischer, Nat. 388 (1997) 756-758.
72. Y. Saito, K. Nishikubo, K. Kawabata, and T. Matsumoto, J. Appl. Phys. 80[5] (1996) 3062-3067.
73. W. Krätschmer, L.D. Lamb, K. Fostiropoulos, and D.R. Huffman, Nat. 347[6291] (1990) 354-358.
74. B.I. Yakobson and R.E. Smalley, Am. Sci. 85[4] (1997) 324-337.
75. T. Guo, P. Nikolaev, A. Thess, D.T. Colbert, and R.E. Smalley, Chem. Phys. Lett. 243[1] (1995) 49-54.
76. A.G. Rinzler, J. Liu, H. Dai, P. Nikolaev, C.B. Huffman, F.J. Rodríguez-Macías, P.J. Boul, A.H. Lu, D. Heymann, D.T. Colbert, R.S. Lee, J.E. Fischer, A.M. Rao, P.C. Eklund, and R.E. Smalley, Appl. Phys. A. 67[1] (1998)

29-37.
77. Y. Zhang and S. Iijima, Appl. Phys. Lett. 75[20] (1999) 3087-3089.
78. W. Zhao, D.N. Seo, H.T. Kim, and I. J. Kim, J. Ceram. Soc. Jpn. 118[1383] (2010) 983-988.
79. K.P. De Jong, and J.W. Geus, Catal. Rev. 42[4] (2000) 481-510.
80. Z.F. Ren, Z.P. Huang, D.Z. Wang, J.G. Wen, J.W. Xu, J.H. Wang, L.E. Calvet, J. Chen, J.F. Klemic, and M.A. Reed, Apply. Phys. Lett. 75[8] (1999) 1086-1088.
81. Z.F. Ren, Z.P. Huang, J.W. Xu, J.H. Wang, P. Bush, M.P. Siegal, and P.N. Provencio, Science 282[5391] (1998) 1105-1107.
82. Z.P. Huang, J.W. Xu, Z.F. Ren, J.H. Wang, M.P. Siegal, and P.N. Provencio, Appl. Phys. Lett. 73[26] (1998) 3845-3847.
83. E.T. Thostenson, Z. Ren, and T.W. Chou, Compos. Sci. Technol. 61[13] (2001) 1899-1912.
84. J. Kong, A.M. Cassell, and H. Dai, Chem. Phys. Lett. 292[4] (1998) 567-574.
85. J.H. Hafner, M.J. Bronikowski, B.R. Azamian, P. Nikolaev, A.G. Rinzler, D.T. Colbert, K.A. Smith, and R.E. Smalley, Chem. Phys. Lett. 296[1] (1998) 195-202.
86. M. Sarikaya and I.A. Aksay, Mater. Res. Soc. Symp. Proc. 255 (1992) 293-307.
87. P. Calvert, MRS Bull. 17[10] (2013) 37-40.
88. M. Sarikaya, Microsc. Res. Tech. 27[5] (1994) 360-375.
89. J.E. Mark and P.D. Calvert, Mater. Sci. Eng. C. 1[3] (1994) 159-173.
90. C.E. Byrne and D.C. Nagle, Carbon 35[2] (1997) 259-266.
91. E. Auer, A. Freund, J. Pietsch, and T. Tacke, Appl. Catal. A. 173[2] (1998) 259-271.
92. J.M. Gatica, A.L. García-Cabeza, M.P. Yeste, R. Marín-Barrios, J.M. González-Leal, G. Blanco, G.A. Cifredo, F.M. Guerra, and H. Vidal, Chem. Eng. J. 209[15] (2016) 174-184.
93. T.X. Fan, T. Hirose, T. Okabe, and D. Zhang, J. Porous Mater. 8[3] (2001) 211-217.
94. D. Mohan, C.U. Pittman, M. Bricka, F. Smith, B. Yancey, J. Mohammad, P.H. Steele, M.F. Alexandre-Franco, V. Gómez-Serrano, and H. Gong, J. Colloid Interface Sci. 310[1] (2007) 57-73.
95. Y. Yao, B. Gao, H. Chen, L. Jiang, M. Inyang, A.R. Zimmerman, X. Cao, L. Yang, Y. Xue, and H. Li, J. Hazard. Mater. 209 (2012) 408-413.
96. D.C. Cruz, in "Production of Bio-coal and Activated Carbon from Biomass" (University of Western Ontario, 2012) p. 20.
97. R. Beigmoradi, A. Samimi, and D. Mohebbi-Kalhori, Beilstein. J. Nanotechnol. 9 (2018) 415-435.
98. K.W. Brown, B. Gessesse, L.J. Butler, and D.L. MacIntosh, Environ. Health Insights. 11 (2017) 1-8.
99. J. Ramírez-Rico, J. Martínez-Fernandez, and M. Singh, Int. Mater. Rev. 62[8] (2017) 465-485.
100. M.H. Ramage, H. Burridge, M. Busse-Wicher, G. Fereday, T. Reynolds, D.U. Shah, G. Wu, L. Yu, P. Fleming, D. Densley-Tingley, J. Allwood, P. Dupreee, P.F. Linden, and O. Scherman, Renewable Sustainable Energy Rev. 68[1] (2017) 333-359.
101. A.J. Panshin and C.D. Zeeuw, in "Textbook of wood technology: structure, identification, properties, and uses of the commercial woods of the United States and Canada" (McGraw-Hill, 1980) p. 83.
102. L.J. Gibson and M.F. Ashby, in "Cellular Solids: Structure and Properties" (Cambridge University Press, 1999) p. 415.
103. R.F. Evert and S.E. Eichhorn in "Esau's Plant Anatomy: Meristems, Cells, and Tissues of the Plant Body: Their Structure, Function, and Development" (Wiley, 2006) p. 296.
104. J.M. Dinwoodie, in "Wood, nature's cellular, polymeric, fibre-composite" (Institute of Metals, 1989) p. 37.
105. H. Yang, R. Yan, H. Chen, D.H. Lee, and C. Zheng, Fuel 86[12] (2007) 1781-1788.
106. J.G. Park, S.Y. Kim, I.S. Han, S.S. Ryu, and I.J. Kim, Int. J. Nanotechnol. 15[6-7] (2018) 460-473.
107. P. Gao, Y. Bai, S. Lin, W. Guo, and H. Xiao, Ceram. Int. 34[8] (2008) 1975-1981.
108. Y.M. Chiang, R.P. Messner, C.D. Terwilliger, and D.R. Behrend, Mater. Sci. Eng. A. 144[1] (1991) 63-74.
109. P. Greil, T. Lifka, and A. Kaindl, J. Eur. Ceram. Soc. 18[14] (1998) 1975-1983.
110. P. Greil, E. Vogli, T. Fey, A. Bezold, N. Popovska, H. Gerhard, and H. Sieber, J. Eur. Ceram. Soc. 22[14] (2002) 2697-2707.
111. M. Singh and D.R. Behrendt, J. Mater. Res. 9[7] (2011) 1701-1708.
112. M. Singh and D. R. Behrendt, Mater. Sci. Eng. A. 194[2] (1995) 193-200.
113. A. Wolfenden, P.J. Rynn, and M. Singh, J. Mater. Sci. 30[21] (1995) 5502-5507.
114. F. Gutierrez-Mora, K.C. Goretta, F.M. Varela-Feria, A.R.A. López, and J.M. Fernández, Int. J. Refract. Met. Hard. Mater. 23[4] (2005) 369-374.
115. M. Presas, J.Y. Pastor, J. Llorca, A.R.A. López, J.M. Fernández, and R.E. Sepúlveda, Int. J. Refract. Met. Hard. Mater. 24[1] (2006) 49-54.
116. M. Presas, J.Y. Pastor, J. Llorca, A.R.A. López, J.M. Fernández, and R.E. Sepúlveda, Scripta. Mater. 53[10] (2005) 1175-1180.
117. M. Presas, J. Pastor, J. Llorca, A. Ramirez de Arellano Lopez, J. Fernández, and R. Sepúlveda Ferrer, Bol. Soc. Esp. Ceram. Vidrio. 44[6] (2005) 363-367.
118. D.J. Lee, J.J. Jang, H.S. Park, Y.C. Kim, K.H. Lim, S.B. Park, and S.H. Hong, Ceram. Int. 38[4] (2012) 3089-3095.
119. G. Hou, Z. Jin, and J. Qian, Mater. Sci. Eng. A. 452[15] (2007) 278-283.
120. V.S. Kaul, K.T. Faber, R. Sepúlveda, A.R.A. López, and J.M. Fernández, Mater. Sci. Eng. A. 428[1] (2006) 225-232.
121. H. Ago, S. Imamura, T. Okazaki, T. Saito, M. Yumura, and M. Tsuji, J. Phys. Chem. B. 109[20] (2005) 10035-10041.
122. K. Hata, D.N. Futaba, K. Mizuno, T. Namai, M. Yumura, and S. Iijima, Science 306[5700] (2004) 1362-1364.
123. R. Andrews, D. Jacques, A.M. Rao, F. Derbyshire, D. Qian, X. Fan, E.C. Dickey, and J. Chen, Chem. Phys. Lett. 303[5] (1999) 467-474.
124. B. Kitiyanan, W.E. Alvarez, J.H. Harwell, and D.E. Resasco, Chem. Phys. Lett. 317[3] (2000) 497-503.
125. D. Ding, J. Wang, Z. Cao, and J. Dai, Carbon 41[3] (2003) 579-582.
126. C.L. Cheung, A. Kurtz, H. Park, and C.M. Lieber, J. Phys. Chem. B. 106[10] (2002) 2429-2433.
127. I. Willems, Z. Kónya, J.F. Colomer, G.V. Tendeloo, N. Nagaraju, A. Fonseca, and J.B. Nagy, AIP. Conf. Proc. 544[1] (2000) 242-245.
128. M. Kumar, and Y. Ando, Carbon 43[3] (2005) 533-540.
129. J.W. Ward, B.Q. Wei, and P.M. Ajayan, Chem. Phys. Lett.

376[5] (2003) 717-725.
130. M. Karthik, A. Vinu, A.K. Tripathi, N.M. Gupta, M. Palanichamy, and V. Murugesan, Microporous Mesoporous Mater. 70[1] (2004) 15-25.
131. M. Kumar and Y. Ando, J. Nanosci. Nanotechnol. 10 (2010) 3739-3758.
132. Y.R. Son, M.K. Kim, S.G. Ryu, and H.S. Kim, ACS. Appl. Mater. Interfaces 10[47] (2018) 40651-40660.
133. S.J. Datta, C. Khumnoon, Z.H. Lee, W.K. Moon, S. Docao, T.H. Nguyen, I.C. Hwang, D. Moon, P. Oleynikov, O. Terasaki, and K.B. Yoon, Science 350[6258] (2015) 302-306.
134. D.H. Lee, and H.S. Kim, Appl. Catal. A. 574 (2019) 71-78.
135. B.M. Weckhuysen and J. Yu, Chem. Soc. Rev. 44[20] (2015) 7022-7024.
136. H.S. Kim and K.B. Yoon, Coord. Chem. Rev. 263[15] (2014) 239-256.
137. G.S. Lee, Y.J. Lee, and K.B. Yoon, J. Am. Chem. Soc. 123[40] (2001) 9769-9779.
138. G. Calzaferri, M. Pauchard, H. Maas, S. Huber, A. Khatyr, and T. Schaafsma, J. Mater. Chem. 12[1] (2002) 1-13.
139. K. Ha, Y.J. Lee, D.Y. Jung, J.H. Lee, and K.B. Yoon, Adv. Mater. 12[21] (2000) 1614-1617.
140. M.L. Liu, B.B. Chen, C.M. Li, and C.Z. Huang, Green. Chem. 21[3] (2019) 449-471.
141. J. Liu, G.E. Fryxell, M. Qian, L.Q. Wang, and Y. Wang, Pure. Appl. Chem. 72[1-2] (2000) 269-279.
142. H. Nishihara and T. Kyotani, Chem. Commun. 54[45] (2018) 5648-5673.
143. W. Zhao, D.N. Seo, J. Gong, S.Y. Kim, and I.J. Kim, J. Ceram. Soc. Jpn. 122[1423] (2014) 187-191.
144. N.P. Stadie, S. Wang, K.V. Kravchyk, and M.V. Kovalenko, ACS. Nano. 11[2] (2017) 1911-1919.
145. K. Nueangnoraj, H. Nishihara, K. Imai, H. Itoi, T. Ishii, M. Kiguchi, Y. Sato, M. Terauchi, and T. Kyotani, Carbon 62 (2013) 455-464.
146. J. Cejka, A. Corma, and S. Zones, in "Zeolites and catalysis: synthesis, reactions and applications" (Wiley-VCH, 2010) p. 109.
147. H. Mori, K. Aotani, N. Sano, and H. Tamon, J. Mater. Chem. 21[15] (2011) 5677-5681.
148. R.J. White, A. Fischer, C. Goebel, and A. Thomas, J. Am. Chem. Soc. 136[7] (2014) 2715-2718.
149. Y. Tao, H. Kanoh, L. Abrams, and K. Kaneko, Chem. Rev. 106[3] (2006) 896-910.
150. W. Zhao, B. Basnet, S. Kim, and I.J. Kim, J. Nanomaterials. 2014 (2014) 1-5.
151. J.P. Hanrahan, A. Donovan, M.A. Morris, and J.D. Holmes, J. Mater. Chem. 17[37] (2007) 3881-3887.
152. P. Gao, M. Wu, B. Li, and Y. Liu, Mater. Res. Bull. 44[3] (2009) 644-648.
153. D. Farrusseng, and A. Tuel, New J. Chem. 40[5] (2016) 3933-3949.
154. A. Choudhary, S.K. Pratihar, and S.K. Behera, RSC Adv. 6[98] (2016) 95897-95902.
155. R. Sun, W. Wang, Y. Wen, and X. Zhang, Nanomaterials 5[4] (2015) 2019-2053.
156. J.G. Park, B. Basnet, S.Y. Kim, I.S. Han, and I.J. Kim, J. Ceram. Proc. Res. 19[3] (2018) 311-315.
157. I.J. Kim, W. Zhao, J.H. Chung, M. Olarin, F. Trandabat, and R.C. Ciobana, J. Ceram. Proc. Res. 11[3] (2010) 303-307.
158. Y.M. Kim, J.H. Chang, and I.J. Kim, J. Cream. Proc. Res. 10[4] (2009) 453-456.
159. K. Flodström, C.V. Teixeira, H. Amenitsch, V. Alfredsson, and M. Lindén, Langmuir 20[12] (2004) 4885-4891.
160. M. Thommes, K. Kaneko, A.V. Neimark, J.P. Olivier, F. Rodriguez-Reinoso, J. Rouquerol, and K.S.W. Sing, Pure. Appl. Chem. 87[9-10] (2015) 1051-1069.
161. K. Sing, Colloids Surf. A. 187 (2001) 3-9.
162. S.V. Boycheva and D.M. Zgureva, Bulg. Chem. Com. A (2016) 110-107.
163. J.G. Park, B. Basneta, S.Y. Kim, S.Y. Kim, and I.J. Kim, J. Cream. Proc. Res. 18[8] (2017) 575-579.
164. G. Che, B.B. Lakshmi, C.R. Martin, E.R. Fisher and R.S. Ruoffr, Chem. Mater. 10[1] (1998) 260-267.
165. S. Mazumder, N. Sarkar, J.G. Park, and I.J. Kim, Mater. Lett. 161[15] (2015) 212-215.
166. W. Zhao, H.S. Kim, H.T. Kim, J. Gong, and I.J. Kim, J. Ceram. Proc. Res. 12[4] (2011) 392-397.
167. R. Beams, L.G. Cancado, and L. Novotny, J. Phys.: Condens. Matter. 27 (2015) 1-26.
168. M.A. Pimenta, G. Dresselhaus, M.S. Dresselhaus, L.G. Cancado, A. Jorio, and R. Saito, Phys. Chem. Chem. Phys. 9 (2007) 1276-1290.
169. F. Zheng, L. Liang, Y. Gao, J.H. Sukamoto, and C.L. Aardahi, Nano. Lett. 2[7] (2002) 729-732.
170. K. An, N Musselwhite, G. Kennedy, V.V. Pushkarev, L.R. Baker, and G.A. Somorjai, J. Colloid Interface Sci. 392[15] (2013) 122-128.
171. J.J. Niu, J.N. Wang, Y. Jiang, L.F. Su, and J. Ma, Microporous Mesoporous Mater. 100[1-3] (2007) 1-5.
172. K.S.W. Sing, D.H. Everett, R.A.W. Haul, L. Moscou, R.A. Pierotti, J. Rouquerol, and T. Simieniewska, Pure Appl. Chem. 57[4] (1985) 603-619.
173. W. Zhao, M.J. Lee, H.T. Kim, and I.J. Kim, Electron. Matter. Lett. 7 (2011) 139-144.
174. W. Zhao, H.T. Kim, and I. J. Kim, J. Ceram. Proc. Res. 13[1] (2012) 81-85.
175. M. Zdrojek, W. Gebicki, C. Jastrzebski, T. Melin, and A. Huczko, Solid State Phenom. 99 (2004) 256-268.
176. M. Sveningsson, R.E. Morjan, O.A. Nerushev, Y. Sato, J. Backstrom, E.E.P. Campbell, and F. Rohmund, Appl. Phys. A. 73[4] (2001) 409-418.
177. S. Karakoulia, L. Jankovic, K. Dimos, D. Gournis, and K. Triantafyllidis, Stud. Surf. Sci. Catal. 158[A] (2005) 391-398.
178. Y. Miyata, K. Mizuno, and H. Kataura, J. Nanomaterials 2011 (2011) 7.
179. J. Kim, J.H. Ha, J.N. Lee, and I.H. Song, J. Korean Ceram. Soc. 53[5] (2016) 548-556.
180. H. Parham, in "Ceramic-Carbon Nanotube Composites and Their Potential Applications" (University of Exeter, 2012) p. 65.
181. C. Mitsakour, C. Housiadas, K. Eleftheriadis, S. Vratolis, C. Helmis, and D. Asimakopoulos, Indoor Air. 17[2] (2007) 143-152.
182. T. Hillie and M. Hlophe, Nat. Nanotechnol. 2[11] (2007) 664-664.
183. R.K. Gautam, S.K. Sharma, S. Mahiya, and M.C. Chattopadhyaya, in "Heavy Metals in Water: Presence, Removal and Safety" (RSC Publishing, 2015) p. 297.
184. A. Züttel, P. Sudan, P. Mauron, T. Kiyobayashi, C. Emmenegger, and L. Schlapbach, Int. J. Hydrogen Energy 27[2] (2002) 203-212.
185. R.S. Barhate and S. Ramakrishna, J. Membr. Sci. 296[1-2] (2007) 1-8.
186. J.H. Wendorff, S. Agarwal, and A. Greiner, in "Electro-spinning : materials, processing, and applications" (Wiley-

VCH, 2012) p. 193.
187. A. Podgórski, A. Bałazy, and L. Gradoń, Chem. Eng. Sci. 61[20] (2006) 6804-6815.
188. S.J. Park and D.G. Lee, Carbon 44[10] (2006) 1930-1935.
189. J.H. Park, K.Y. Yoon, H. Na, Y.S. Kim, J. Hwang, J. Kim, J.B. Kim, and Y.H. Yoon, Sci. Total. Environ. 409[19] (2011) 4132-4138.
190. S.T. Mostafavi, M.R. Mehrnia, and A.M. Rashidi, Desalin. 238[1-3] (2009) 271-280.
191. H.R. Rashid and S.F. Ralph, Nanomater. 7[5] (2017) 99-127.
192. M.T. Bankole, A.S. Abdulkareen, I.A. Mohammed, S.S. Ochigbo, J.O. Tijani, O.K. Abubakre, and W.D. Roos, Sci. Rep. 9[1] (2019) 4475-4493.
193. A. Gadhave and J. Waghmare, Int. J. Chem. Sci. Appl. 5[2] (2015) 56-67.
194. T. Akasaka and F. Watari, Acta Biomater. 5[2] (2009) 607-612.
195. Y.H. Li, S. Wang, Z. Luan, J. Ding, C. Xu, and D. Wu, Carbon 41[5] (2003) 1057-1062.
196. J. Yang, B. Hou, J. Wang, B. Tian, J. Bi, N. Wang, X. Li, and X. Huang, Nanomater. 9[3] (2019) 424-463.
197. C. Lu and C. Liu, Chem. Technol. Biotechnol. 81[12] (2006) 1932-1940.
198. Z.C. Di, J. Ding, X.J. Peng, Y.H. Li, Z.K. Luan, and J. Liang, Chemosphere 62[5] (2006) 861-865.
199. G. Luo, H. Yao, M. Xu, X. Cui, W. Chen, R. Gupta, and Z. Xu, Energy Fuels 24[1] (2009) 419-426.
200. A. Schierz and H. Zänker, Environ. Pollut. 157[4] (2009) 1088-1094.
201. G.P. Rao, C. Lu, and F. Su, Sep. Purif. Technol. 58[1] (2007) 224-231.
202. Y.H. Li, Z. Di, J. Ding, D. Wu, Z. Luan, and Y. Zhu, Water Res. 39[4] (2005) 605-609.
203. C. Lu, H. Chiu, and C. Liu, Ind. Eng. Chem. Res. 45[8] (2006) 2850-2855.
204. X. Gui, J. Wei, K. Wang, A. Cao, H. Zhu, Y. Jia, Q. Shu, and D. Wu, Adv. Mater. 22[5] (2010) 617-621.
205. C. Lee and S. Baik, Carbon 48[8] (2010) 2192-2197.
206. Z. Chen, L. Zhang, Y. Tang, and Z. Jia, Appl. Surf. Sci. 252[8] (2006) 2933-2937.